International Journal of Heat and Mass Transfer 220 (2024) 124998

Contents lists available at ScienceDirect

International Journal of Heat and Mass Transfer

journal homepage: www.elsevier.com/locate/ijhmt

Prediction technique for flow boiling heat transfer and critical heat flux in both microgravity and Earth gravity via artificial neural networks (ANNs)

Issam Mudawar *, Steven J. Darges, V.S. Devahdhanush

Purdue University Boiling and Two-Phase Flow Laboratory (PU-BTPFL), School of Mechanical Engineering, Purdue University, 585 Purdue Mall, West Lafayette, IN 47907, USA

ARTICLE INFO

Keywords:
Flow boiling
Microgravity
Machine learning
Neural network
Heat transfer
Critical heat flux

ABSTRACT

This study is part of the Flow Boiling and Condensation Experiment (FBCE) and utilizes flow boiling data collected in both microgravity onboard the International Space Station (ISS) and Earth gravity at different channel orientations. The goal is to develop a prediction technique for heat transfer and critical heat flux (CHF) for flow boiling in both microgravity and Earth gravity using artificial neural networks (ANNs). The working fluid, n-perfluorohexane or FC-72, flows through a rectangular channel of 114.6 mm heated length, 2.5 mm heated width, and 5.0 mm unheated height with either one or two walls heated. The consolidated FBCE database for heat transfer coefficient comprises 29,226 datapoints spanning a mass velocity of 173 – 3200 kg/m^{2}s, pressure of 102 – 238 kPa, subcooling of 0 – 44°C, and thermodynamic equilibrium quality of -0.60 – 0.95 (spanning from highly subcooled to high-quality saturated boiling). Following a statistical analysis of various input parameters relevant to flow boiling and optimization of key model parameters, a fully connected feed-forward ANN is developed to predict Nu_{tp}. It predicts the entire test database with an overall mean absolute error (MAE) of just 7.99% with consistent and accurate predictions in each subset. Similarly, 641 CHF datapoints from FBCE were consolidated into a database spanning a mass velocity of 99 – 3212 kg/m^{2}s, inlet pressure of 97 – 239 kPa, inlet subcooling of 0 – 46°C, inlet thermodynamic equilibrium quality of -0.61 – 0.86, and CHF values of 4 – 54 W/cm^2. A separate ANN is developed by following the same methodology as heat transfer, and it predicts dimensionless CHF, Bo_{CHF}, with an overall MAE of just 12.05%. Existing seminal correlations are assessed for subsets of the two consolidated FBCE databases, and the ANNs are shown to have better accuracies in each subset of the database. The ANNs' high prediction accuracy, in conjunction with their ability to predict physical parametric trends in previously unseen data, shows their potential as prediction tools for both heat transfer and CHF for flow boiling in microgravity and Earth gravity.

1. Introduction

1.1. Two-phase systems in microgravity

Two-phase systems are a prime contender for thermal management in future space missions [1]. Compared to single-phase systems that solely rely on sensible heat, two-phase provides superior heat transfer performance by utilizing the fluid's latent heat of vaporization. Moreover, two-phase systems can handle larger cooling loads while being lighter and more compact, a benefit for many aerospace applications. Nevertheless, designing two-phase systems for space vehicles is a challenging task. Variations in body force alter system performance, such as heat transfer and flow characteristics, from that observed in Earth gravity (g_e), which most design tools are developed for. Consequently, dependable microgravity databases are required to develop and validate available design tools for space applications.

Numerous researchers have dedicated experiments to obtain boiling data in microgravity. Typically, short durations of microgravity are achieved during terrestrial experiments via drop towers, sounding rockets or ballistic missiles, or parabolic flights. These methods provide meaningful microgravity data, but each has its drawbacks. Drop towers provide a high quality of microgravity but for very short durations [2]. Sounding rockets and parabolic flights provide longer durations of microgravity but are prone to fluctuations in the level of g, known as g-jitter [3], which can artificially augment heat transfer performance.

To circumvent these drawbacks, experiments can be conducted onboard the International Space Station (ISS) to obtain long-duration,

* Corresponding author.
E-mail address: mudawar@ecn.purdue.edu (I. Mudawar).

https://doi.org/10.1016/j.ijheatmasstransfer.2023.124998
Received 24 September 2023; Received in revised form 10 November 2023; Accepted 20 November 2023
Available online 27 November 2023

Nomenclature

A_c	channel cross-sectional area, [m^2]
b	bias
Bd	Bond number, $g(\rho_f - \rho_g)D^2/\sigma$
Bd_θ	orientation-specific Bond number, $g\cos\theta(\rho_f - \rho_g)D^2/\sigma$
Bo	Boiling number, $q''_w/(Gh_{fg})$
C	constant
c_p	specific heat, [J/(kg.K)]
Ca	capillary number, $G\nu/\sigma$
D	diameter, [m]
D_e	equivalent heated diameter, $4A_c/P_h$, [m]
D_h	hydraulic diameter, [m]
E	loss
F	convective boiling correction factor
$f(v)$	activation function
Fr	Froude number, $G^2/(\rho^2 gD)$
Fr_θ	orientation-specific Froude number, $G^2/(\rho_f^2 g\sin\theta D)$
G	mass velocity, [kg/(m^2s)]
g	gravitational acceleration, [m/s^2]
g_e	gravitational acceleration on Earth, [m/s^2]
μg_e	microgravity, [m/s^2]
H	height of channel, [m]
h	heat transfer coefficient, [W/(m^2K)]
h_{fg}	latent heat of vaporization, [J/kg]
Ja^{**}	modified Jacob number, $c_{p,f}\Delta T_{sub}/h_{fg}$
k	thermal conductivity, [W/(m.K)]
L	length, [m]
La	Laplace number, $\sigma\rho D/\mu$
M_w	molecular weight, [kg/kmol]
n	exponent; mini-batch size
N	number of data points
Nu	Nusselt number, hD/k
P	perimeter, [m]
p	pressure, [Pa]
p_r	reduced pressure, p/p_{crit}
Pr	liquid Prandtl number, $c_p\mu/k$
q''	heat flux, [W/m^2]
r	Pearson's correlation coefficient
Re	liquid only Reynolds number, GD/μ
S	nucleate boiling suppression factor
T	temperature, [°C]
ΔT_{sat}	fluid subcooling, $T_w - T_{sat}$, [°C]
ΔT_{sub}	fluid subcooling, $T_{sat} - T_f$, [°C]
t	target value
U	velocity, [m/s]
v	weighted sum of inputs and bias at a neuron
W	width of channel, [m]
w_i	weight
We	Weber number, $G^2D/(\rho\sigma)$
x	flow quality
x_e	thermodynamic equilibrium quality, $\frac{h-h_f}{h_{fg}}$
x_i	input
X_{tt}	turbulent-turbulent Lockhart-Martinelli parameter, $\left(\frac{\mu_f}{\mu_g}\right)^{0.1}\left(\frac{1-x}{x}\right)^{0.9}\left(\frac{\rho_g}{\rho_f}\right)^{0.5}$
y	output

Greek symbols

θ	orientation angle of channel, [°]
μ	dynamic viscosity; mean, [Pa.s]
ξ_{30}	percentage of datapoints predicted within ±30% error, [%]
ξ_{50}	percentage of datapoints predicted within ±50% error, [%]
ρ	density, [kg/m^3]
σ	surface tension; standard deviation, [N/m]
φ	probability value

Subscripts

CHF	critical heat flux
d	development
D_e	calculated $D = D_e$
e	exit
exp	experimental
f	saturated liquid; bulk fluid
fo	liquid only
g	saturated vapor
go	vapor only
h	heated
i	index (= 1, 2, 3, …)
in	inlet
nb	nucleate boiling
out	outlet
$pred$	predicted
sat	saturation
sp	single-phase
sub	subcooling
tp	two-phase
w	wall, wetted
wa	heated wall (= $w1$ or $w2$)

Acronyms

ANN	artificial neural network
BGD	batch gradient descent
CHF	critical heat flux
FBCE	flow boiling and condensation experiment
FBM	flow boiling module
ISS	international space station
MAE	mean absolute error (%)
MBGD	mini-batch gradient descent
MST	mission sequence testing
nPFH	n-Perfluorohexane
RMSE	root mean square error (%)
SGD	stochastic gradient descent

stable microgravity data. In 2011, the Microheater Array Boiling Experiment [3] and the Nucleate Pool Boiling Experiment [4] collected microgravity pool boiling data onboard the ISS. Both investigations revealed a decrease in heat transfer and a significant deterioration in the critical heat flux (CHF) in microgravity when compared to g_e. Flow boiling experiments were performed onboard the ISS by researchers in collaboration with the Japanese Aerospace eXploration Agency with nPFH through a 4-mm-diameter copper heated tube and transparent glass tube onboard the ISS from 2017–2019 [5].

In 2022, a group of researchers supported by the European Space Agency outlined experiments onboard the ISS from 2019 and 2021 called the Multiscale Boiling Project [6]. Four different categories of experiments were performed including pool boiling, shear flow, pool boiling in the presence of an electric field, and shear flow in the presence of an electric field. These experiments were done to investigate the contact line behavior of bubbles, growth of bubbles, influence of an

electric field, and influence of shear flow. In the absence of external forces, bubbles grew larger with increasing heat flux and decreasing subcooling. Introducing shear flow caused bubbles to depart from the nucleation site and slide along the heated surface. Similarly, pool boiling in an electric field promoted stable bubble detachment in microgravity, but bubbles lifted away perpendicular from the heated surface. Increasing the strength of the electric field caused the detachment of small bubbles. During the combination of shear flow and an electric field, bubbles either lift-off or slide along the heated surface depending on the relative magnitudes of the electric field and the flow inertia.

In 2023, researchers associated with the Institute of Fluid Mechanics of Toulouse and Airbus Defense and Space in Friedrichshafen, Germany, published an article outlining a future experiment called CoSmo (Compact Small Scale Convection Loop) for implementation on the ISS [7]. The primary objective of this study is to investigate the effects of gravity on flow patterns and heat transfer during flow boiling of nPFH in a 6-mm-diameter copper heated tube and borosilicate glass adiabatic tubing. Thus far, preliminary experiments have been performed for vertical upflow in Earth gravity and onboard a parabolic flight. Experiments were performed with low mass velocities of 20 – 150 kg/m^{2}s, pressures of 0.5 – 1.5 bar, subcoolings of 0 – 10 K, and inlet qualities of 0.0 – 0.8.

The Flow Boiling and Condensation Experiment (FBCE), a collaborative effort between researchers at the Purdue University Boiling and Two-Phase Flow Laboratory and the NASA Glenn Research Center, aims to explore flow boiling and condensation in microgravity at an unprecedented scale by performing extensive experiments onboard the ISS. Prior to the ISS experiments, a fundamental understanding of gravity's influence on flow boiling and condensation was developed via experiments conducted in g_e at different flow orientations [8] and in brief periods of microgravity achieved during parabolic flights [9]. Technical insights from terrestrial experiments led to refinements of the FBCE system culminating in the *flight* FBCE system, which can be utilized for both flow boiling and condensation experiments by connecting the appropriate test module. In early 2021, the flight system equipped with the Flow Boiling Module (FBM) underwent a final round of ground tests called Mission Sequence Testing (MST) [10]. MST was conducted in the vertical upflow orientation and consisted of a subset of the parameters to be covered during ISS experiments, especially the extremes. Based on the preliminary experiments up to and including MST, new correlations were developed for both subcooled flow boiling heat transfer [11] and CHF [12].

In August 2021, the FBCE system was launched to the ISS and installed in the Fluid Integrated Rack. From February 2022 until July 2022, a variety of flow boiling experiments were performed, yielding a large microgravity database for flow boiling heat transfer and CHF. Experimental results and analysis of trends have already been reported for subcooled inlet with single- [13] and double-sided heating [14], and liquid-vapor mixture inlet with single- and double-sided heating [15]. The corresponding CHF results were further explored in detail along with prediction tools (mechanistic model and correlation) for subcooled [16] and two-phase inlet [17].

1.2. Prediction of two-phase heat transfer coefficient

To capitalize on expertise gained from experiments in μg_e and g_e, the collected data is used to develop predictive tools which can be incorporated during the design and analysis of thermal systems. Numerous correlations are available in the literature for various applications spanning different fluids, heating configurations, and operating conditions. Correlations are typically designed for either saturated flow boiling ($x_e \geq 0$) or subcooled flow boiling ($x_e < 0$) with select correlations capable of handling both. However, as detailed in reviews of existing correlations for flow boiling heat transfer [18,19], a definitive method for predicting h for flow boiling has not been established, but a few common functional forms are prominent. Enhancement type [20, 21] correlations follow the functional form of

$$h_{tp} = Ch_{sp}, \tag{1}$$

where h_{tp} can be determined from h_{sp} and a multiplier, C, to account for boiling, which varies in form.

Asymptotic models [22,23] assume h_{tp} is comprised of components attributed to nucleate boiling and forced convection and follow the form,

$$h_{tp}^n = (S \times h_{nb})^n + \left(F \times h_{sp}\right)^n. \tag{2}$$

Superposition models are a special subset of asymptotic models with $n = 1$, and was first proposed by Chen [24] as

$$h_{tp} = (S \times h_{nb}) + \left(F \times h_{sp}\right). \tag{3}$$

The multipliers in front of each component are conventionally called the nucleate boiling suppression factor, S, and the convective boiling correction factor, F, and are respectively used to regulate the relative influence of nucleate boiling and convective heat transfer. Researchers have proposed numerous methods to determine each term [25,26].

Predominant mechanism models assume h_{tp} can be approximated by the maximum of h determined for each mechanism separately, typically either nucleate or convective boiling [27]. In some cases, nucleate boiling is preemptively considered the dominant mechanism and correlations do not consider other mechanisms [28]. Other researchers have proposed different correlations for h_{tp} based on local conditions. Models based on flow pattern [29] combine knowledge of flow patterns within a channel, such as the local wetted perimeter of the channel, with empirical correlations to develop a model with a more physical basis. In a similar vein, hybrid models propose transition criteria to capture different heat transfer mechanisms and determine the appropriate correlation to be employed [30].

One of the earliest fully subcooled correlations was proposed by McAdams et al. [31] and assumes a simple power-law relation,

$$q = C\Delta T_{sat}^n. \tag{4}$$

This form was adopted in a few other early subcooled flow boiling correlations [32,33], but correlations of this form are typically restricted in their applicability to broad operating ranges and fluids other than water.

1.3. Application of machine learning for thermal systems

The ever-growing capability and availability of computational resources favors machine learning algorithms to tackle complex problems. Machine learning has become a commonplace in predicting the performance of various thermal systems such as building energy consumption [34], ground source heat pumps [35], gas turbines [36], internal combustion engines [37], heat exchangers [38], and heat sinks [39]. Machine learning has also been incorporated in predicting the fundamental heat transfer performance of nanofluids [40] and porous media [41]. However, most relevant to the present study is the adaptation of machine learning methods for predicting heat transfer in two-phase systems.

An artificial neural network (ANN) was developed by Guanghui *et al.* [42] to capture the effect of flow instability on CHF. They trained models for either natural circulation or pumped loops under low pressure conditions with inputs of conventional parameters such as average mass flow rate, pressure, inlet subcooling, and the ratio of heated length to diameter. To account for instabilities, both the amplitude and the period of mass flow rate oscillations were included as inputs. The output of the model was a non-dimensional factor describing the ratio between CHF with and without oscillations. Their model predicted 85% of the training data within ±10% relative error.

Wang et al. [43] formed a consolidated database featuring flow boiling h data for R-22, R-134A, R-407C, and R-410A in horizontal

smooth tubes. The authors developed an ANN with a single hidden layer to predict h. They choose the inputs to their model by non-dimensionalizing the typical inputs of h correlations. The authors refit existing correlations to their database. Regardless, their ANN outperformed each correlation with a mean deviation of 13.0%.

Cong et al. [44] showed the applicability of neural networks in predicting CHF for forced convective boiling on a heated surface with impinging jets. Their ANN consisted of a single hidden layer, used conventional dimensionless terms that influence CHF as inputs, and accurately predicted boiling number for their database. The authors additionally used a genetic algorithm to propose a correlation based on the inputs to their ANN but found their ANN to be more accurate.

Zaidi [45] utilized support vector regression to predict h for boiling in a thermosyphon reboiler. The model was trained with a consolidated database of natural circulation heat transfer data featuring 8 different fluids. They used the logarithm of nondimensional terms affecting h to predict the logarithm of Nu and showed all their test data was predicted within 20% of the experimental data.

An ANN for predicting h for saturated flow boiling in mini-/micro-channels was presented by Qiu et al. [46]. Their network was trained from a consolidated database of nearly 17,000 data points featuring 16 different fluids, different channel geometries, and a broad range of operating conditions. They tested different combinations of dimensional and dimensionless inputs while optimizing their model. Finally, dimensionless inputs were selected for better generality, regardless of dimensional inputs achieving slightly better predictions. They tested the capability of their ANN to predict unseen data by eliminating individual databases from the consolidated database used for training. After retraining, the model proved adept at predicting data outside the training data set.

Longo et al. [47] developed an ANN for predicting h for refrigerants inside a brazed plate heat exchanger. Adding a second hidden layer insignificantly improved the model so only a single hidden layer was used. Increasing the number of nodes within the hidden layer asymptotically decreased the error of the model, and 12 nodes were selected in the final model. The minimum number of nodes to reach sufficient accuracy was used as the final model. Their final ANN showed better predictive capability than available theoretical models, and accurately predicted data that is not well captured by other predictive models such as low-pressure refrigerants at high reduced pressures.

A neural network to estimate pool boiling h for dielectric liquids, refrigerants, and water on porous surfaces was developed by Sajjad et al. [48]. The influence of the combination of surface material and liquid on heat transfer was captured by including parameters of both as inputs to the model. The authors tested different network architectures and settled on a network with three hidden layers. Their preferred model was capable of predicting a wide range of operating conditions for different fluids with an overall mean absolute error of 5.74%.

Zhou et al. [49] tested different machine learning algorithms to predict h for a condensing flow in mini-/micro-channels via a consolidated database. Their optimized ANN consisted of 15 consecutively narrowing hidden layers from 150 to 10 neurons and outperformed three decision tree-based models (Random Forest, Adaptive Boost, and Extreme Gradient Boosting). They used a variety of dimensionless groups as inputs to predict h and outperformed previously developed generalized correlations. The authors showed their models could predict individual datasets that were intentionally left out of training, provided the working fluid was still present within the training data.

Zhu *et al.* [50] trained 2 ANNs, one for flow boiling heat transfer, and the other for condensation heat transfer. Each network consisted of 7 hidden layers with the 7 most relevant dimensionless groups, determined by SOBOL sensitivity analysis for either flow boiling or condensation. Using the appropriate ANN, the authors predicted their database of flow boiling and condensation of R-134a in mini-channels with serrated fins with respective mean absolute relative deviations of 11.41% and 6.06%. However, the authors showed extrapolating the ANN to conditions outside the scope of the training data resulted in unreliable predictions, and the mean absolute relative deviation exceeded 120%.

Cho et al. [51] explored the effects of non-condensable gas on the heat transfer of a free-falling condensing film. They consolidated a database of condensing water vapor with various geometric parameters, operating conditions, and mass fraction of either non-condensable air or nitrogen. A new correlation was developed by nonlinear regression to fit the present database, and it outperformed those available in the literature. However, the performance of empirical correlations, including those which were fit to the present database, was trumped by their trained ANN. The authors optimized their ANN by testing architectures of 2 – 10 uniform layers with 2 – 40 nodes in each layer and settled on 6 layers containing 26 nodes per layer. Inputs to their model included the natural log of operating conditions, and properties of the working fluid and non-condensable gas. Their model predicted the entire database within ±50% error.

Predictive models for flow condensation heat transfer in horizontal tubes were developed by Nie et al. [52] using different machine learning models including K-nearest neighbors, ANN, convolutional neural network, random forest, and extreme gradient boosting algorithms. They tested four different combinations of input parameters to train their models: (i) experimental parameters, (ii) experimental parameters with thermophysical properties, (iii) dimensionless groups, and (iv) a consolidated group containing all other parameters. Each model performed satisfactorily, but the authors favored the dimensionless input parameters for better scaling when comparing with other databases. The neural networks and extreme gradient boosting algorithm were the best-performing models, outperforming K-nearest neighbors and random forest. However, the extreme gradient boosting model performed the best for predicting datasets that were excluded from training.

Qiu et al. [53] proposed a systematic approach to optimize ANN models for predicting flow boiling h in mini-/micro-channel heatsinks. Using the same database as [46], an ANN with improved accuracy was achieved by (1) selecting inputs utilized in previous physics-based correlations, (2) including additional inputs which show statistical significance in influencing h, and (3) performing a thorough grid search to optimize the model's hyperparameters and network architecture.

1.4. Objectives of present study

The primary goal of the Flow Boiling and Condensation Experiment (FBCE), is to obtain crucial flow boiling and condensation data in microgravity, which can be used to develop and verify design tools. The present study capitalizes on the unique and extensive database for microgravity flow boiling collected onboard the ISS. The ISS microgravity database is combined with a pre-launch database to form a consolidated FBCE heat transfer database comprised of data obtained in microgravity and Earth gravity at different orientations. The consolidated database is used to train an ANN for predicting flow boiling heat transfer in microgravity. Development of the ANN involves a statistical analysis of inputs relevant to flow boiling and optimization of key model parameters. Then, another ANN is developed to predict flow boiling CHF using a consolidated FBCE-CHF database. Both the ANNs are assessed with respect to accuracy, predicted trends, and comparison to available correlations.

2. Methodology

2.1. Description of database

All data consolidated in the present database was collected during FBCE with the Flow Boiling Module (FBM), presented in Fig. 1. FBM is formed by three polycarbonate plates stacked between two aluminum support plates and bolted together. The middle polycarbonate plate contains a 5.0 mm × 2.5 mm ($H \times W$) rectangular channel. Two opposite

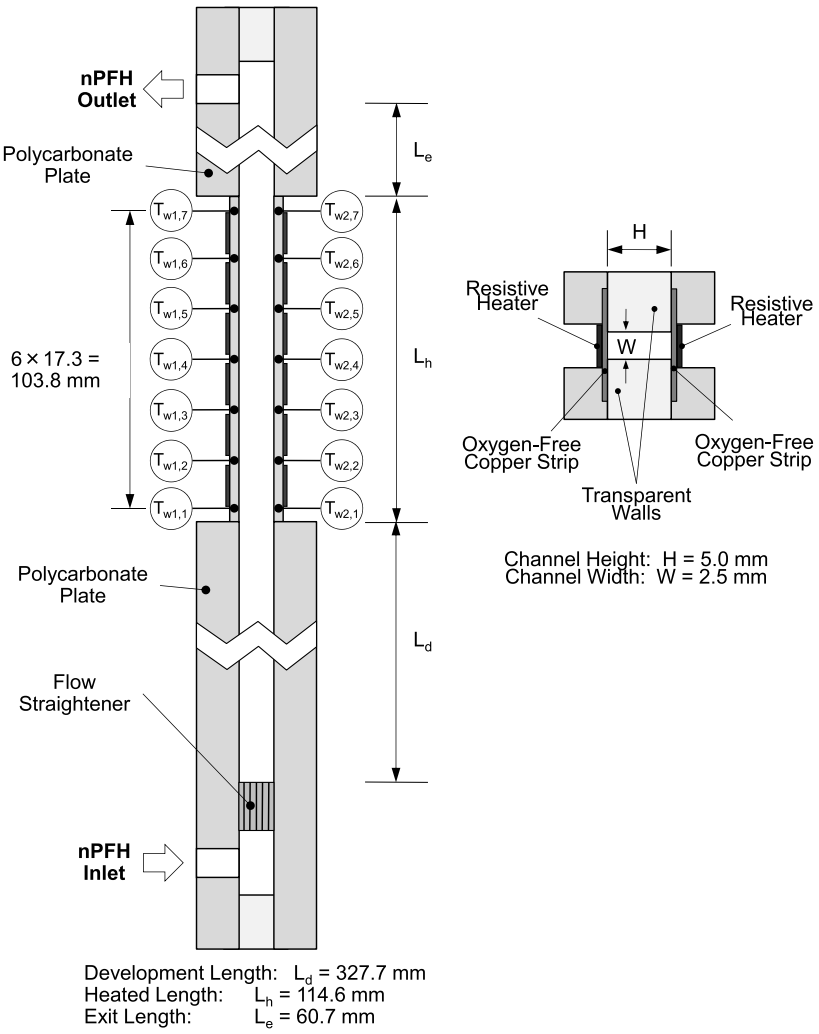

Fig. 1. Schematic diagrams of streamwise and cross-sectional views of the experimental flow boiling module. The module's dimensions are included along with placements of the wall temperature thermocouples in the heated strips.

heated walls are formed by copper strips, 114.6 mm long, 15.5 mm wide, and 1.04 mm thick, inserted into the polycarbonate. Heat is supplied to the copper walls by six thick-film resistive heaters attached to the back side of each copper strip, opposite the flow channel. Copper-strip temperatures are recorded by thermocouples placed between successive heaters. The entire 327.7 mm entrance length, side walls of the 114.6 mm heated length, and entire 60.7 mm exit length are adiabatic and are formed by insulating polycarbonate. Both upstream and downstream of the heated length, fluid temperature and pressure are recorded via thermocouples inserted directly into the flow and absolute pressure transducers, respectively.

The database includes flow boiling heat transfer data obtained during

(i) ground tests in 2015 [54] featuring different orientations (vertical upflow, vertical downflow, and horizontal flow with bottom and top wall heating), single- and double-sided heating, and saturated inlet conditions,
(ii) ground tests in 2016 [55] featuring different orientations (vertical upflow, vertical downflow and horizontal flow), double-sided heating, and subcooled liquid and saturated two-phase inlet,
(iii) ground tests during MST in 2021 [10,56] featuring vertical upflow, single- and double-sided heating, and subcooled liquid and saturated two-phase inlet conditions, and
(iv) experiments onboard the ISS in 2022 [13–15] featuring μg_e, single- and double-sided heating, and subcooled liquid and saturated two-phase inlet conditions.

The consolidated FBCE heat transfer database contains 29,226 datapoints of local flow parameters (G, p, T, ΔT_{sub}, and x_e), heated wall measurements (T_w and q''_w) and calculated two-phase heat transfer coefficient (h_{tp}) obtained during flow boiling. Flow quality (x) is a measure of the relative amount of vapor in the channel and is approximated assuming equilibrium conditions as

$$x = \begin{cases} 0, & x_e < 0 \\ x_e, & 0 \le x_e \le 1 \\ 1, & x_e > 1 \end{cases}. \tag{5}$$

The ranges of relevant parameters of the database are presented in Table 1. Additional details regarding the experimental setup, operating procedure, data processing, and uncertainty are provided in the original publications [10,13–15,54–56].

2.2. Artificial neural networks

ANNs are black box models capable of mapping complex, nonlinear, relationships between large quantities of inputs and outputs [57,58]. They have gained widespread popularity in various fields, including

Table 1
Summary of consolidated FBCE heat transfer coefficient database.

	Single-sided Horizontal Bottom	Horizontal Top	Vertical Up	Vertical Down	μg_e	Double-sided Horizontal Bottom	Horizontal Top	Vertical Up	Vertical Down	μg_e	Overall
Number of data points, N	930	648	1278	688	4668	1093	1103	3420	1795	13,603	29,226
Mass velocity, G [kg/m^{2}s]	192.52 – 2028.09	190.21 – 2037.91	179.93 – 3199.98	199.34 – 2031.17	179.97 – 3200.10	182.85 – 2438.82	182.85 – 2438.82	172.79 – 3200.00	195.18 – 2317.96	179.36 – 3200.01	172.79 – 3200.10
Pressure, p [kPa]	113.97 – 178.53	113.51 – 176.21	108.48 – 174.99	115.35 – 176.76	113.47 – 176.57	102.16 – 195.21	102.16 – 195.21	107.48 – 228.26	114.99 – 238.44	114.79 – 196.63	102.16 – 238.44
Fluid temperature, T [°C]	60.64 – 74.96	60.52 – 74.52	35.87 – 74.29	61.01 – 74.62	25.09 – 74.59	24.70 – 75.90	24.70 – 75.90	29.02 – 75.58	27.10 – 76.12	25.52 – 78.23	24.70 – 78.23
Fluid Subcooling, ΔT_{sub} [°C]	0.00	0.00	0.00 – 27.42	0.00	0.00 – 43.70	0.00 – 36.33	0.00 – 36.33	0.00 – 40.29	0.00 – 38.03	0.00 – 43.44	0.00 – 43.70
Equilibrium Quality, x_e	0.005 – 0.756	0.005 – 0.711	-0.375 – 0.777	0.005 – 0.751	-0.603 – 0.921	-0.486 – 0.758	-0.486 – 0.758	-0.560 – 0.865	-0.514 – 0.861	-0.599 – 0.952	-0.603 – -0.952
Approximated Flow Quality, x	0.005 – 0.756	0.005 – 0.711	0.000 – 0.777	0.005 – 0.751	0.000 – 0.921	0.001 – 0.758	0.000 – 0.758	0.000 – 0.865	0.000 – 0.861	0.000 – 0.952	0.000 – 0.952
Wall heat flux q''_w [W/m^2]	28,828 – 206,940	18,720 – 221,769	25,312 – 480,917	18,720 – 221,769	20,359 – 550,738	18,104 – 474,821	18,720 – 499,901	17,969 – 494,884	24,641 – 456,610	20,363 – 517,965	17,969 – 550,738
Heated wall temperature, T_w [°C]	64.92 – 84.34	62.05 – 98.60	60.50 – 117.38	63.57 – 81.48	64.47 – 121.15	57.45 – 91.00	57.46 – 98.86	59.74 – 115.61	64.10 – 114.15	65.70 – 121.61	57.45 – 121.61
Heat transfer coefficient h [W/m^{2}K]	4197.1 – 22,364.8	2278.5 – 29,902.9	1571.3 – 29,401.9	7083.8 – 32,648.8	1334.5 – 17,744.6	2819.7 – 21,963.4	2665.4 – 29,631.4	1426.3 – 28,251.7	3247.3 – 31,706.2	1070.4 – 23,610.3	1070.4 – 32,648.8

security, science, engineering, medical research, agriculture, finance, banking, and numerous others. This popularity is attributed to their exceptional accuracy, fast processing speed, fault tolerance, low latency, high performance, large capacity, and scalability [59]. In the 1940s, McCulloch and Pitts [60] proposed the mathematical modeling of a neuron as a switch, which is either active or inactive depending on the weighted sum of its inputs. An example of a neuron, which serves as the fundamental computational unit of an ANN, is depicted in Fig. 2(a), where x_i are the inputs to the neuron, w_i are the corresponding weights applied to x_i, and b is the bias. Each neuron passes the weighted sum of its inputs and a bias, v, through a non-linear activation function, $f(v)$, to yield an output, y. Common activation functions include the Sigmond function, hyperbolic tangent function, and rectified linear unit (ReLu) function [61]. The ReLu activation function is preferable for mitigating the vanishing gradient problem (where the gradient goes to 0), accelerating convergence of gradient descent algorithms [62], and is calculated as

$$f(v) = \begin{cases} v, & v \geq 0 \\ 0, & v < 0 \end{cases}, \tag{6}$$

Fig. 2(b) depicts the architecture of a fully connected feed-forward neural network. The network is comprised of three types of layers. No computations are performed in the first layer, called the input layer, and its size is dictated by the number of input parameters. Following the input layer are hidden layers. A network contains one or more hidden layers, each containing any number of neurons. The final layer, called the output layer, yields the desired output parameters of the network. In a fully connected neural network, each neuron in a given layer is connected to each neuron in the previous and following layers. Depending on the types of connections, networks are classified as either feed-forward or recurrent. In feed-forward networks, information propagates from the input layer towards the output layer, such that the outputs of one layer serve as the inputs for the following layer, and there is no feedback to previous layers. Networks with connections that provide feedback to previous layers and send information towards the input layer are called recurrent networks. Only feed-forward networks are explored in this paper.

The back propagation algorithm, developed by Rumelhart et al. [63], is a commonly used gradient descent technique for training multi-layer, feed-forward neural networks. This algorithm enables the tuning of

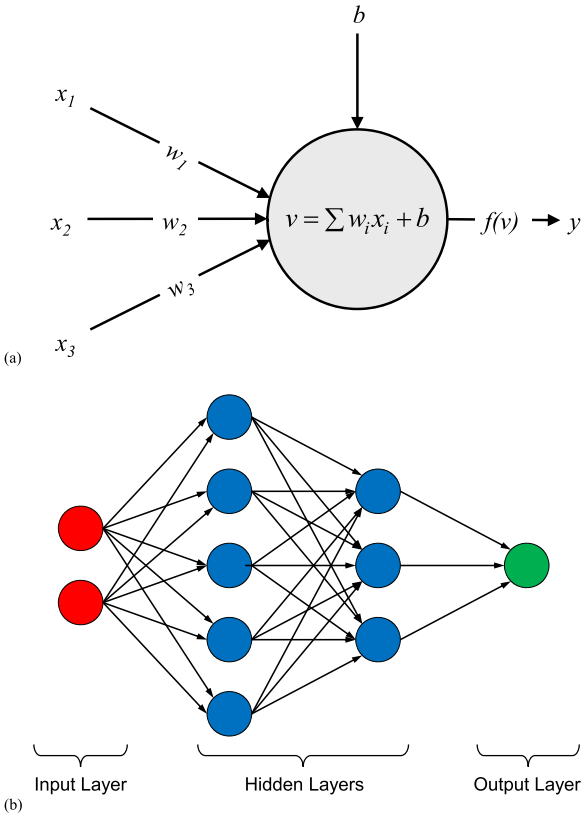

Fig. 2. Schematics displaying (a) the operation of a single neuron including the inputs, x_i, corresponding weight applied to each input, w_i, bias, b, input to activation function, v, activation function, $f(v)$, and output, y, and (b) the connectivity between neurons in a fully connected feed-forward network.

weights and biases within the network to minimize the loss function, which is used to measure error. Half of the Mean Squared Error (MSE) of the outputs is commonly employed as the loss function for regression problems, and, with a single output, it is calculated as

$$E = \frac{1}{2}\sum_{i=1}^{n}(y_i - t_i)^2, \tag{7}$$

where E is the loss, y_i and t_i are the predicted and target output of observation i, respectively, and n is the total number of observations in each iteration. The gradient of the loss function is explicitly calculated at the output layer and propagated backward through the network towards the input layer. The weights and biases are then updated with the gradient of loss with respect to the local weight via the selected learning rule.

The present study employs the learning algorithm called Adam [64], which is well suited for convergence of multilayer neural networks, to regulate the updating of weights and biases. Updating occurs at the end of each iteration; however, n is a selected value which can be varied to optimize and accelerate convergence. The extreme values of n are either 1, corresponding to Stochastic Gradient Descent (SGD), or N, corresponding to Batch Gradient Descent (BGD) [65]. During SGD, the weights and biases are updated for each observation, and there are N iterations per *epoch*, which corresponds to a single passing of the entire training dataset. Updates are frequent in SGD, resulting in a computationally expensive process and fluctuations in loss. The model is updated once per epoch in BGD, resulting in stable but possibly suboptimal convergence. The Mini-Batch Gradient Descent (MBGD) utilizes intermediate values of n and balances the robustness of SGD and the stability of BGD. During MBGD, the number of iterations per epoch is obtained by truncating N/n, and the remaining observations are skipped. The observations used in each iteration can be shuffled at the end of each epoch, such that the same data is not excluded from training.

One prevalent issue with ANNs is overtraining, where the ANN model becomes overly specific to the data used to train it. To mitigate overtraining, the database is randomly divided into three subsets. The *training data* accounts for 70% of the entire database and is used during the training process. The *testing data* accounts for 15% of the database and is used to assess the accuracy of the model after training is completed. The remaining 15% of the database is used for *validation* during training. The loss of the validation data is calculated at the end of each iteration. Once the loss of the validation does not improve for a selected number of training iterations, termed the *validation patience*, training is stopped to prevent the model from losing generality to data not used during training. In the present study, the validation patience is indicated as a number of epochs.

2.3. Model development

2.3.1. Selection of input parameters

A compilation of possible input parameters is formed by assessing various flow boiling heat transfer coefficient correlations available in literature. Correlations are conventionally developed for either subcooled ($x_e < 0$) or saturated ($x_e \geq 0$) flow boiling, due to the different mechanisms and trends observed in each regime [66]. Tables 2 and 3 present selected seminal correlations developed for large, consolidated databases, their relevant input parameters, and corresponding dimensionless groups, for subcooled and saturated flow boiling heat transfer, respectively. The overarching characteristics of the input parameters describe the heated surface condition, flow inertia, state of the fluid, liquid film near the wall, impact of body force, and channel geometry. The input parameters from all listed correlations can be consolidated as

$$h_{tp} = f\left(\begin{matrix} q''_w, D_h, D_e, P_w, P_h, T_w, \Delta T_{sat}, G, U, p, T_f, \Delta T_{sub}, x_e, \ldots \\ x, \rho_f, \rho_g, c_{p,f}, \mu_f, \mu_f|_{T_w}, k_f, T_{sat}, \sigma, h_{fg}, p_{crit}, M_w, g, \theta \end{matrix}\right). \tag{8}$$

The comprehensive list contains parameters that are irrelevant or redundant in describing h_{tp} for the present database. In order to develop an explicit model for h_{tp}, one of either q''_w or T_w should be included as an input. For the present database, experiments were performed by controlling the wall heat flux, hence q''_w is preserved as an input and T_w is removed. In the same vein, parameters dependent on wall temperature, such as those describing the liquid film, are eliminated as possible inputs. The effect of orientation, θ, is quantified by capturing the effects of gravity parallel and perpendicular to the flow as $g.\sin\theta$ and $g.\cos\theta$, respectively. The definition of θ employed in [12] is adopted in the present study where horizontal bottom wall heating, vertical upflow, horizontal top wall heating, and vertical downflow correspond to $\theta = 0°$, 90°, 180°, and 270°, respectively.

The relation between different parameters, including the dependent variable, h_{tp}, is examined via Pearson's correlation coefficient (r), which assesses the linear dependence between any two variables. For any two parameters A and B, r is defined as

$$r(A,B) = \frac{1}{N-1}\sum_{i=1}^{N}\left(\frac{A_i - \mu_A}{\sigma_A}\right)\left(\frac{B_i - \mu_B}{\sigma_B}\right), \tag{9}$$

where r approaching 1, −1, or 0, respectively indicates a positive linear correlation, a negative linear correlation, or no correlation, between variables. The r for each pair of parameters is depicted in Fig. 3 by both the color gradient indicating the value of r and the size of the circle increasing with the magnitude of r (*i.e.*, strong and weak correlations are represented by large and small circles, respectively). Inspection of the relationship between different variables reveals the following:

(1) Parameters such as D_h, P_f, and M_w are constant in the present database and are independent of other variables.
(2) Fluid properties exhibit significant correlation, either positively or negatively, to pressure due to nPFH being the one and only fluid.
(3) Certain parameters are redundant and describe similar physical attributes affecting h_{tp}, such as G and U, T_f and ΔT_{sub}, as well as D_e and P_h.

Parameters that show no dependence and fluid properties are removed from consideration as inputs for the model. Furthermore, G, ΔT_{sub}, and D_e are selected to describe inertia, subcooling, and channel geometry, respectively, and U, T_f, and P_h are eliminated. After eliminating unnecessary parameters, the dependency of h_{tp} for the present database can be written as

$$h = f(q''_w, D_e, G, p, \Delta T_{sub}, x, x_e, g, g.\sin\theta, g.\cos\theta) \tag{10}$$

An *F-Test* is a type of hypothesis test to determine the probability that the response values grouped by predictor variables come from populations with the same mean. A *p-value* (probability value), φ, gives the probability that the null hypothesis, which assumes the means are unrelated, is true and the variable is statistically insignificant. *Null hypothesis* is generally rejected when the p-value is less than 0.05 [73,74]. Fig. 4(a) depicts the importance of each predictor as $-\ln(\varphi)$, where values over 3 correspond to p-values less than 0.05, indicating statistical importance. Clearly, D_e is significantly less important than the other parameters considered. However, mimicking conventional correlations and separating the subcooled and saturated flow boiling heat transfer data, the influence of input parameters in each regime can be observed. Fig. 4(b) focuses on subcooled boiling, and D_e becomes a key variable where the heated perimeter strongly influences the fluid's subcooling, impacting heat transfer performance. On the other hand, the influence of gravity perpendicular to the heated wall, $g.\cos\theta$, is more pronounced during saturated boiling in Fig. 4(c). This is attributed to the buoyancy causing stratified flow at low flow rates during horizontal flow in saturated flow boiling, where vapor production is significant.

An ANN is first developed for subcooled flow boiling and saturated flow boiling, separately. Training is performed with the MATLAB Deep Learning Toolbox [75]. Prior to training, the inputs are standardized by subtracting their means and dividing by their standard deviations. The He initializer, which was developed for improved convergence with

Table 2
Select seminal correlations for subcooled flow boiling and their relevant parameters.

Author(s) (Year)	Correlation, Input Parameters, and Dimensionless Groups	Applicability Information	Prediction Accuracy for Entire Consolidated Database
Papell (1963) [67]	$\frac{Nu_{tp}}{Nu_{sp}} = 90\left(\frac{q''_w}{h_{fg}\rho_g U}\right)^{0.7}\left(\frac{h_{fg}}{c_{p,f}\Delta T_{sub}}\right)^{0.84}\left(\frac{\rho_g}{\rho_f}\right)^{0.756}$ (11a) $\frac{Nu_{tp}}{Nu_{sp}} = 90Bo^{0.7}Ja^{**-0.84}\left(\frac{\rho_g}{\rho_f}\right)^{0.056}$ (11b) $Nu_{sp} = 0.021\mathrm{Re}_{fo}^{0.8}\mathrm{Pr}_f^{0.4}$ (11c) Input Parameters: $h_{tp} = f\left(\begin{matrix}q''_w, U, \Delta T_{sub}, D, h_{fg}, \rho_g, \rho_f, \ldots \\ c_{p,f}, \mu_f, k_f\end{matrix}\right)$ (11d) Dimensionless groups: $Nu_{tp} = f\left(Bo, Ja^{**}, \frac{\rho_g}{\rho_f}, \mathrm{Re}_f, \mathrm{Pr}_f\right)$ (11e)	• Geometry: uniformly heated tube • Fluids: distilled water, ammonia • Consolidated database of 306 data points • Recommended/validated range: p = 110.32 – 13,789.52 kPa U = 0.41 – 62.22 m/s ΔT_{sub} = 3.33 – 186.67°C $q''_w = 42.49 \times 10^3 - 91.52 \times 10^6$ W/m^2	MAE = 74.51%
Badiuzzaman (1967) [68]	$\frac{Nu_{tp}}{Nu_{sp}} =$ $C_1\left[\left(\frac{q''_w}{h_{fg}\rho_g U}\right)\left(\frac{h_{fg}}{c_{p,f}\Delta T_{sub}}\right)^{1.2}\left(\frac{\rho_g}{\rho_f}\right)^{1.08}\left(\frac{\Delta T_{sub}}{T_{sat}}\right)^{0.6}\right]^{C_2}$ (12a) $\frac{Nu_{tp}}{Nu_{sp}} = C_1\left[BoJa^{**-1.2}\left(\frac{\rho_g}{\rho_f}\right)^{1.08}\left(\frac{\Delta T_{sub}}{T_{sat}}\right)^{0.6}\right]^{C_2}$ (12b) Water: $C_1 = 178$, $C_2 = 0.75$ Organic fluids: $C_1 = 759$, $C_2 = 0.89$ (used in this study) $Nu_{sp} = 0.021\mathrm{Re}_f^{0.8}\mathrm{Pr}_f^{0.4}$ (12c) Input Parameters: $h_{tp} = f\left(\begin{matrix}q''_w, U, \Delta T_{sub}, T_{sat}, D, h_{fg}, \rho_g, \rho_f, \ldots \\ c_{p,f}, \mu_f, k_f\end{matrix}\right)$ (12d) Dimensionless groups: $Nu_{tp} = f\left(Bo, Ja^{**}, \frac{\Delta T_{sub}}{T_{sat}}, \frac{\rho_g}{\rho_f}, \mathrm{Re}_f, \mathrm{Pr}_f\right)$ (12e)	• Geometry: Flow over horizontal rectangular strip • Fluids: Water, ethanol, isopropanol • Database of 260 data points • Recommended/validated range: U = 0.26 – 1.22 m/s ΔT_{sub} = 27.78 – 70.00°C $q''_w \leq 1.66 \times 10^6$ W/m^2	MAE = 48.83%
Moles & Shaw (1972) [21]	$\frac{Nu_{tp}}{Nu_{sp}} =$ $78.5\left(\frac{q''_w}{h_{fg}\rho_g U}\right)^{0.67}\left(\frac{h_{fg}}{c_{p,f}\Delta T_{sub}}\right)^{0.5}\left(\frac{\rho_g}{\rho_f}\right)^{0.7}\left(\frac{c_{p,f}\mu_f}{k_f}\right)^{0.46}$ (13a) $\frac{Nu_{tp}}{Nu_{sp}} = 78.5Bo^{0.67}Ja^{**-0.5}\left(\frac{\rho_g}{\rho_f}\right)^{0.03}\mathrm{Pr}_f^{0.46}$ (13b) $Nu_{sp} = 0.027\mathrm{Re}_f^{0.8}\mathrm{Pr}_f^{1/3}\left(\frac{\mu_f}{\mu_f\vert_{T_w}}\right)^{0.14}$ (13c) Input Parameters: $h_{tp} = f\left(\begin{matrix}q''_w, U, \Delta T_{sub}, D, h_{fg}, \rho_g, \rho_f, \ldots \\ c_{p,f}, \mu_f, \mu_f\vert_{T_w}, k_f\end{matrix}\right)$ (13d) Dimensionless groups: $Nu_{tp} = f\left(Bo, Ja^{**}, \frac{\rho_g}{\rho_f}, \mathrm{Re}_f, \mathrm{Pr}_f, \frac{\mu_f}{\mu_f\vert_{T_w}}\right)$ (13e)	• Geometry: vertical upflow in a circular tube, vertical upflow in rectangular channel, horizontal flow over a heated strip in a rectangular channel, vertical upflow through a channel made of a heated circular tube placed along the center of a square channel • Fluids: water, ethanol, isopropanol, n-butanol, ammonia, aniline, hydrazine • Consolidated database of 664 data points • Recommended/validated range: D_h = 4.6 – 16.2 mm U = 0.03 – 62.22 m/s p = 101.35 – 13,789.52 kPa ΔT_{sub} = 2.78 – 277.78°C $q''_w = 72.51 \times 10^3 - 91.42 \times 10^6$ W/m^2	MAE = 60.58%
Gungor & Winterton (1986) [25]	$q''_w = h_{tp}(T_w - T_f) = Eh_{sp}(T_w - T_f) + Sh_{nb}(T_w - T_{sat})$ (14a) $h_{tp} = Eh_{sp} + Sh_{nb}\frac{\Delta T_{sat}}{(T_w - T_f)}$ (14b) $\frac{h_{sp}D}{k_f} = Nu_{sp} = 0.023\mathrm{Re}_f^{0.8}\mathrm{Pr}_f^{0.4}$ (14c) $h_{nb} = 55p_r^{0.12}(-\log_{10}p_r)^{-0.55}M_w^{-0.5}q''^{0.67}_w$ (14d) $E = 1$ (14e) $S = (1 + 1.15 \times 10^{-6}E^2\mathrm{Re}_f^{1.17})^{-1}$ (14f) For horizontal tubes with $Fr_{fo} \leq 0.05$: $E = E.Fr_{fo}^{0.1-2Fr_{fo}}$ (14 g) $S = S.Fr_{fo}^{0.5}$ (14 h) Input Parameters: $h_{tp} = f\left(\begin{matrix}q''_w, G, T_f, \Delta T_{sub}, T_w, \Delta T_{sat}, D, h_{fg}, \rho_g, \rho_f, \ldots \\ c_{p,f}, \mu_f, k_f, p, p_{crit}, M_w, g\end{matrix}\right)$ (14i) Dimensionless groups: $Nu_{tp} = f\left(Bo, Ja^{**}, \frac{\Delta T_{sat}}{(T_w - T_f)}, \mathrm{Re}_f, \mathrm{Pr}_f, Fr, p_r\right)$ (14j)	• Geometry: vertical and horizontal tubes and annuli • Fluids: ethylene glycol, water, refrigerants • Consolidated database of over 4300 data points • Recommended/validated range: D_h = 2.95 – 32.0 mm G = 12.40 – 61,518.00 kg/m^{2}s ΔT_{sub} = 0.00 – 173.70°C $q''_w = 350.00 - 91.53 \times 10^6$ W/m^2	MAE = 33.13%
Liu & Winterton (1991) [22]	$q''_w = h_{tp}(T_w - T_f) =$ $\{(Eh_{sp}(T_w - T_f))^2 + (Sh_{nb}(T_w - T_{sat}))^2\}^{0.5}$(15a) $h_{tp} = \left\{(Eh_{sp})^2 + \left(\frac{Sh_{nb}\Delta T_{sat}}{(T_w - T_f)}\right)^2\right\}^{0.5}$ (15b) $\frac{h_{sp}D}{k_f} = Nu_{sp} = 0.023\mathrm{Re}_f^{0.8}\mathrm{Pr}_f^{0.4}$ (15c) $h_{nb} = 55p_r^{0.12}(-\log_{10}p_r)^{-0.55}M_w^{-0.5}q''^{0.67}_w$ (15d) $E = 1$ (15e)	• Geometry: horizontal and vertical tubes and annuli • Fluids: water, refrigerants, ethylene glycol, ethanol, n-butanol • Consolidated database of 5193 data points • Recommended/validated range: D_h = 2.95 – 32.0 mm G = 12.4 – 8179.3 kg/m^{2}s ΔT_{sub} = 0.0 – 173.7°C ΔT_{sat} = 0.2 – 62.3°C	MAE = 74.51%

(*continued on next page*)

Table 2 (*continued*)

Author(s) (Year)	Correlation, Input Parameters, and Dimensionless Groups	Applicability Information	Prediction Accuracy for Entire Consolidated Database
	$S = (1 + 0.055E^{0.1}\mathrm{Re}_f^{0.16})^{-1}$ (15f) For horizontal tubes with $Fr_{fo} \leq 0.05$: $E = E.Fr_{fo}^{0.1-2Fr_{fo}}$ (15 g) $S = S.Fr_{fo}^{0.5}$ (15 h) Input Parameters: $h_{tp} = f\left(\begin{matrix} q''_w, G, T_f, \Delta T_{sub}, T_w, \Delta T_{sat}, D_e, h_{fg}, \rho_g, \rho_f, \cdots \\ c_{p,f}, \mu_f, k_f, p, p_{crit}, M_w, g \end{matrix}\right)$ (15i) Dimensionless groups: $Nu_{tp} = f\left(Bo, Ja^{**}, \frac{\Delta T_{sat}}{(T_w - T_f)}, \mathrm{Re}_{fo}, \mathrm{Pr}_f, Fr, p_r\right)$ (15j)	$q''_w = 348.9 - 2.62 \times 10^6$ W/m^2 $x = 0.000 - 0.948$ $p_r = 0.0023 - 0.895$ $Pr_f = 0.83 - 9.1$ $Fr = 2.66 \times 10^{-4} - 2240$ $Re_f = 568.9 - 8.75 \times 10^5$	
Shah (2017) [69]	$q''_w = h_{tp}(T_w - T_f) = \begin{cases} \frac{\psi_0 h_{sp}(\Delta T_{sat} - 1.65\Delta T_{sub}^{-0.44})}{0.67}, & PDB \\ \psi_0 h_{sp} \Delta T_{sat}. & FDB \end{cases}$ (16a) $\psi_0 = \begin{cases} 230Bo^{0.5}, & Bo > 0.3 \times 10^{-4} \\ 1 + 46Bo^{0.5}, & Bo < 0.3 \times 10^{-4} \end{cases}$ (16b) $\frac{h_{sp}D}{k_f} = Nu_{sp} = 0.023\mathrm{Re}_{fo}^{0.8}\mathrm{Pr}_f^{0.4}$ (16c) Input Parameters: $h_{tp} = f\left(\begin{matrix} q''_w, G, T_f, \Delta T_{sub}, T_w, \Delta T_{sat}, D_e, \cdots \\ h_{fg}, c_{p,f}, \mu_f, k_f \end{matrix}\right)$ (16d) Dimensionless groups: $Nu_{tp} = f\left(Bo, \frac{\Delta T_{sub}}{\Delta T_{sat}}, \mathrm{Re}_{fo}, \mathrm{Pr}_f\right)$ (16e)	• Geometry: horizontal and vertical flow in channels of various geometries and annuli of different heating configurations • Fluids: water, refrigerants, chemicals • Consolidated database of 1340 data points • Recommended/validated range: $D_h = 0.176 - 22.8$ mm $G = 59 - 31{,}500$ kg/m^{2}s $\Delta T_{sub} = 0.0 - 165$°C $p_r = 0.0046 - 0.922$ $Bo = 0.53 \times 10^{-4} - 91.2 \times 10^{-4}$ $Pr_f = 0.83 - 9.1$ $Bd = 0.025 - 7100$ $Re_{fo} = 375 - 1.27 \times 10^6$ $Pe = 631 - 1.11 \times 10^6$	MAE = 42.36%
Devahdhanush & Mudawar (2022) [11]	$\frac{h_{tp}}{h_{sp}} = 312.8\left(\frac{q''_w}{Gh_{fg}}\right)^{0.769}\left(0.1 + \frac{c_{p,f}\Delta T_{sub}}{h_{fg}}\right)^{-0.632}$ (17a) $\frac{Nu_{tp}}{Nu_{sp}} = 312.8Bo^{0.769}(0.1 + Ja^{**})^{-0.632}$ (17b) $\frac{h_{sp}D}{k_f} = Nu_{sp} = 0.023\mathrm{Re}_{fo}^{0.8}\mathrm{Pr}_f^{0.4}$ (17c) Input Parameters: $h_{tp} = f\left(\begin{matrix} q''_w, G, U, \Delta T_{sub}, D, h_{fg}, \rho_g, \rho_f, \cdots \\ c_{p,f}, \mu_f, k_f \end{matrix}\right)$ (17d) Dimensionless groups: $Nu_{tp} = f(Bo, Ja^{**}, \mathrm{Re}_{fo}, \mathrm{Pr}_f)$ (17e)	• Geometry: rectangular channel heated on 1 or 2 opposite heated walls, different orientations • Fluids: nPFH and FC-72 • Consolidated database of 3009 data points • Recommended/validated range: $D_h = 3.33$ mm $G = 172.79 - 3200.00$ kg/m^{2}s $p = 102.16 - 238.44$ kPa $\Delta T_{sub} = 0.13 - 34.93$°C $q''_w = 38.0 \times 10^3 - 482.7 \times 10^3$ W/m^2 $p_r = 0.059 - 0.137$ $Bo = 1.65 \times 10^{-4} - 187.6 \times 10^{-4}$ $Pr_f = 5.65 - 7.4$ $Re_{fo} = 966.72 - 26{,}883.66$ $Pe = 631 - 1.11 \times 10^6$ $\rho_f/\rho_g = 48.38 - 117.66$	MAE = 30.08%

rectified linear activations such as ReLu [76], is used to initialize weights. Relevant input parameters and a preliminary set of training options employed to train each model, which are chosen from the default parameters recommended for Adam [64] and those utilized in the studies outlined in Section 1.3, are presented in Table 4. In the present study, network architectures are built such that the final hidden layer, preceding the output layer, always has 10 neurons. Each layer has 10 more neurons than the following, so a network with 5 hidden layers has an architecture of {50–40–30–20–10} neurons between the input and output layers. Another example is a network with 10 hidden layers would have a hidden layer architecture of {100–90–80–70–60–50–40–30–20–10}.

The results of each model are presented in Figs. 5(a) and 5(b). Each model only uses the parameters relevant for its own flow boiling regime. They are capable of accurately predicting h_{tp} for their respective testing database with MAEs of 6.31% and 11.70% for subcooled and saturated flow boiling, respectively. To assess if a single model can be used for both subcooled and saturated flow boiling, another ANN is trained for the entire database using the same parameters in Table 4. Fig. 5(c) depicts results for the ANN trained with the entire database, which predicts the testing data with an MAE of 9.53%. The accuracy of the overall ANN lies between those of the models specifically trained for subcooled and saturated flow boiling. Interestingly, the ANN trained with the entire database predicts the subcooled and saturated subset of the database with MAEs of 6.63% and 11.79%, respectively, nearly identical to the ANNs trained specifically for each subset.

2.3.2. Model refinement

A common technique to improve the generality of a correlation or ANN is to rely on dimensionless numbers that describe the relative magnitude of key parameters to one another. Based on the dimensionless groups observed in Tables 2 and 3, the dependency of h_{tp} expressed in Eq. (10) can be non-dimensionalized as

$$Nu_{tp} = f\left(Bo, \frac{D_e}{D_h}, Re, We, p_r, \frac{\rho_g}{\rho_f}, \mathrm{Pr}, Ja^{**}, x, x_e, X_{tt}, Fr, Bd, \frac{g}{g_e}\right). \quad (24)$$

Numerous variations of each dimensionless group could be utilized as inputs for the ANN, however not all will significantly improve the model. To optimize those selected as inputs for the final model, a variety of models are trained using the training parameters listed in Table 4 and different combinations of dimensionless groups. A comprehensive list of inputs considered is included in Table 5. A subset of noteworthy results and their corresponding input parameters are further included in Table 6. Using only *Bo*, Nu_{tp} is predicted with a MAE of 47.46%. Subcooling and quality are added in group 2, and the MAE improved to 31.45%. The model is then drastically improved by incorporating the effect of G in group 3. Continuing to add other parameters such D_e/D_h and ρ_g/ρ_f, the MAE of the model is decreased to 11.82%. Inclusion of additional terms to describe pressure, such as p_r, only provides minor improvement and is deemed unnecessary. The influence of both gravity

Table 3
Select seminal correlations for saturated flow boiling and their relevant parameters.

Author(s) (Year)	Correlation, Input Parameters, and Dimensionless Groups	Applicability Information	Prediction Accuracy For Entire Consolidated Database
Gungor & Winterton (1986) [25]	$q''_w = h_{tp}(T_w - T_f) = Eh_{sp}(T_w - T_f) + Sh_{nb}(T_w - T_{sat})$ (18a) $h_{tp} = Eh_{sp} + Sh_{nb}\frac{\Delta T_{sat}}{(T_w - T_f)}$ (18b) $\frac{h_{sp}D}{k_f} = Nu_{sp} = 0.023\mathrm{Re}_f^{0.8}\mathrm{Pr}_f^{0.4}$ (18c) $h_{nb} = 55p_r^{0.12}(-\log_{10}p_r)^{-0.55}M_w^{-0.5}q''^{0.67}_w$ (18d) $E = 1 + 24000Bo^{1.16} + 1.37\left(\frac{1}{X_{tt}}\right)^{0.86}$ (18e) $S = (1 + 1.15\times10^{-6}E^2\mathrm{Re}_{fo}^{1.17})^{-1}$ (18f) For horizontal tubes with $Fr_{fo} \le 0.05$: $E = E.Fr_{fo}^{0.1-2Fr_{fo}}$ (18g) $S = S.Fr_{fo}^{0.5}$ (18h) Input Parameters: $h_{tp} = f\left(\begin{matrix} q''_w, G, T_f, \Delta T_{sub}, T_w, \Delta T_{sat}, D, h_{fg}, \rho_g, \rho_f, \dots \\ c_{p,f}, \mu_f, k_f, p, p_{crit}, M_w, g \end{matrix}\right)$ (18i) Dimensionless groups: $Nu_{tp} = f\left(Bo, Ja^{**}, \frac{\Delta T_{sat}}{(T_w - T_f)}, \mathrm{Re}_{fo}, \mathrm{Pr}_f, Fr, p_r\right)$ (18j)	• Geometry: vertical and horizontal tubes and annuli • Fluids: ethylene glycol, water, refrigerants • Consolidated database of over 4300 data points • Recommended/validated range: D_h = 2.95 – 32.0 mm G = 12.40 – 61,518.00 kg/m^{2}s ΔT_{sub} = 0.00 – 173.70°C q''_w = 350.00 – 91.53 × 10^6 W/m^2	MAE = 223.40%
Liu & Winterton (1991) [22]	$q''_w = h_{tp}(T_w - T_f) =$ $\{(Eh_{sp}(T_w - T_f))^2 + (Sh_{nb}(T_w - T_{sat}))^2\}^{0.5}$(19a) $h_{tp} = \left\{(Eh_{sp})^2 + \left(\frac{Sh_{nb}\Delta T_{sat}}{(T_w - T_f)}\right)^2\right\}^{0.5}$ (19b) $\frac{h_{sp}D}{k_f} = Nu_{sp} = 0.023\mathrm{Re}_f^{0.8}\mathrm{Pr}_f^{0.4}$ (19c) $h_{nb} = 55p_r^{0.12}(-\log_{10}p_r)^{-0.55}M_w^{-0.5}q''^{0.67}_w$ (19d) $E = \left(1 + x\mathrm{Pr}_f\left(\frac{\rho_f}{\rho_g} - 1\right)\right)^{0.35}$ (19e) $S = (1 + 0.055E^{0.1}\mathrm{Re}_f^{0.16})^{-1}$ (19f) For horizontal tubes with $Fr_{fo} \le 0.05$: $E = E.Fr_{fo}^{0.1-2Fr_{fo}}$ (19g) $S = S.Fr_{fo}^{0.5}$ (19h) Input Parameters: $h_{tp} = f\left(\begin{matrix} q''_w, G, T_f, \Delta T_{sub}, T_w, \Delta T_{sat}, D_e, h_{fg}, \rho_g, \rho_f, \dots \\ c_{p,f}, \mu_f, k_f, p, p_{crit}, M_w, g \end{matrix}\right)$ (19i) Dimensionless groups: $Nu_{tp} = f\left(Bo, Ja^{**}, \frac{\Delta T_{sat}}{(T_w - T_f)}, \mathrm{Re}_{fo}, \mathrm{Pr}_f, Fr, p_r\right)$ (19j)	• Geometry: horizontal and vertical tubes and annuli • Fluids: water, refrigerants, ethylene glycol, ethanol, n-butanol • Consolidated database of 5193 data points • Recommended/validated range: D_h = 2.95 – 32.0 mm G = 12.4 – 8179.3 kg/m^{2}s ΔT_{sub} = 0.0 – 173.7°C ΔT_{sat} = 0.2 – 62.3°C q''_w = 348.9 – 2.62 × 10^6 W/m^2 x = 0.000 – 0.948 p_r = 0.0023 – 0.895 Pr_f = 0.83 – 9.1 Fr = 2.66 × 10^{-4} – 2240 Re_f = 568.9 – 8.75 × 10^5	MAE = 52.97%
Tran *et al.* (1996) [70]	$h_{tp} = 8.4\times10^5(Bo^2We_{fo})^{0.3}\left(\frac{\rho_g}{\rho_f}\right)^{0.4}$ (20a) Input Parameters: $h_{tp} = f(q''_w, G, h_{fg}, D, \rho_f, \sigma, \rho_g)$ (20b) Dimensionless groups: $Nu_{tp} = f\left(Bo, We_{fo}, \frac{\rho_g}{\rho_f}\right)$ (20c)	• Geometry: horizontal, circular and rectangular channels • Fluids: R12 and R113 • Consolidated database of 296 data points • Recommended/validated range: D_h = 2.4 – 2.92 mm G = 44 – 832 kg/m^{2}s ΔT_{sat} = 1.2 – 18.2°C q''_w = 3.6 × 10^3 – 129 × 10^3 W/m^2 p_r = 0.045 – 0.2 Bo = 2.0 × 10^{-4} – 23.0 × 10^{-4}	MAE = 79.43%
Li & Wu (2010) [71]	$Nu_{tp} = 334Bo^{0.3}(Bd\mathrm{Re}_f^{0.36})^{0.4}$ (21a) Input Parameters: $h_{tp} = f(q''_w, G, h_{fg}, D, \rho_f, \rho_g\sigma, g, x, \mu_f, k_f)$ (21b) Dimensionless groups: $Nu_{tp} = f(Bo, Bd, \mathrm{Re}_f)$ (21c)	• Geometry: horizontal and vertical, circular and rectangular, mini-/micro- single- and multi-channel • Fluids: water, refrigerants, CO_2, ethanol, propane, and FC77 • Consolidated database of 3744 data points • Recommended/validated range: D_h = 0.16 – 3.1 mm	MAE = 56.11%
Kim & Mudawar (2013) [23]	$h_{tp} = (h_{nb}^2 + h_{cb}^2)^{0.5}$ (22a) $\frac{Nu_{nb}}{Nu_{sp}} = 2345\left(Bo\frac{P_h}{P_f}\right)^{0.70}p_R^{0.38}(1 - x_e)^{-0.51}$ (22b) $\frac{Nu_{nb}}{Nu_{sp}} = 5.2\left(Bo\frac{P_h}{P_f}\right)^{0.08}We_{fo}^{-0.54} + 3.5\left(\frac{1}{X_{tt}}\right)^{0.94}\left(\frac{\rho_g}{\rho_f}\right)^{0.25}$ (22c) $Nu_{sp} = 0.023\mathrm{Re}_f^{0.8}\mathrm{Pr}_f^{0.4}$ (22d) Input Parameters: $h_{tp} = f\left(\begin{matrix} q''_w, G, h_{fg}, P_h, P_f, p, p_{crit}, x, D, \dots \\ \rho_f, \sigma, \mu_f, \mu_g, \rho_g, k_f \end{matrix}\right)$ (22e) Dimensionless groups: $Nu_{tp} = f\left(Bo, \frac{P_h}{P_f}, p_R, x, We_{fo}, X_{tt}, \frac{\rho_g}{\rho_f}\right)$ (22f)	• Geometry: horizontal and vertical, circular and rectangular, mini-/micro-, single- and multi-channels • Fluids: water, refrigerants, FC-72, and CO_2 • Consolidated database of 10,805 data points • Recommended/validated range: D_h = 0.19 – 6.5 mm G = 19 – 1608 kg/m^{2}s x = 0.0001 – 0.999 p_r = 0.005 – 0.69 Pr_f = 0.9 – 6.7 Re_{fo} = 57 – 49,820	MAE = 72.30%

(*continued on next page*)

Table 3 (*continued*)

Author(s) (Year)	Correlation, Input Parameters, and Dimensionless Groups	Applicability Information	Prediction Accuracy For Entire Consolidated Database
Fang et al. (2017) [72]	$Nu_{tp} = F_f M_w^{-0.18} Bo^{0.98} Fr_{fo}^{0.48} Bd^{0.72} \left(\frac{\rho_f}{\rho_g}\right)^{0.29} \left[\ln\left(\frac{\mu_f\vert_{T_f}}{\mu_f\vert_{T_w}}\right)\right]^{-1} Y$ (23a) $Y = \begin{cases} 1, & p_r \le 0.43 \\ 1.38 - p_r^{1.15}, & p_r > 0.43 \end{cases}$ (23b) F_f = 1850, Tabulated for different fluids Input Parameters: $h_{tp} = f\left(\begin{matrix} M_w, q''_w, G, h_{fg}, \rho_f, \rho_g, D, g, \sigma, \dots \\ \mu_f, \mu_f\vert_{T_w}, p, p_{crit}, k_f \end{matrix}\right)$ (23c) Dimensionless groups: $Nu_{tp} = f\left(Bo, Fr_{fo}, Bd, \frac{\rho_f}{\rho_g}, \frac{\mu_f\vert_{T_f}}{\mu_f\vert_{T_w}}, p_r\right)$ (23d)	• Geometry: horizontal, vertical, and inclined, circular and rectangular, single- and multi-channels • Fluids: water, CO_2, nitrogen, ammonia, refrigerants • Consolidated database of 24,442 data points • Recommended/validated range: D_h = 0.137 – 32.0 mm G = 10 – 1782 kg/m^{2}s q''_w = 200 – 4.8 × 10^6 W/m^2 x = 0.0001 – 0.999 p_r = 0.0045 – 0.93 Pr_f = 0.9 – 6.7 Re_f = 4.9 – 1.69 × 10^5 Re_g = 7.9 – 5.13 × 10^5	MAE = 55.55%

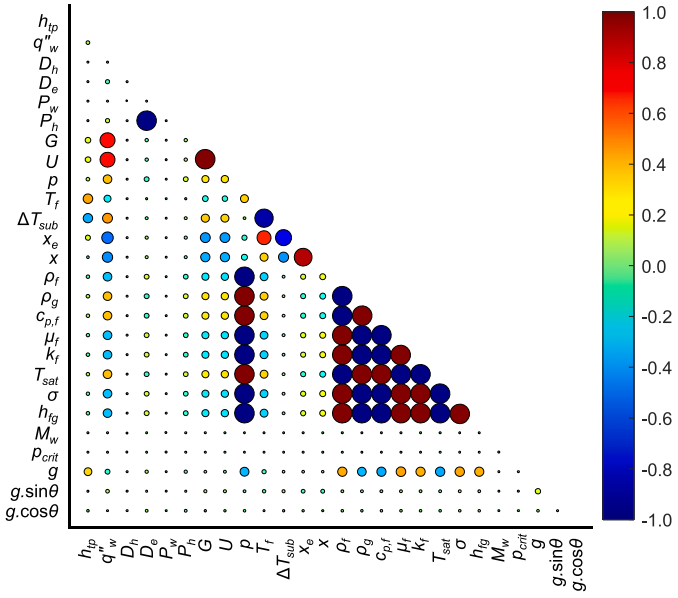

Fig. 3. Pearson's correlation coefficients (r) for the comprehensive list of input parameters: two-phase heat transfer coefficient (h_{tp}), wall heat flux (q''_w), hydraulic diameter (D_h), equivalent heated diameter (D_e), wetted perimeter (P_w), heated perimeter (P_h), mass velocity (G), fluid velocity (U), pressure (p), bulk fluid temperature (T_f), degree of subcooling (ΔT_{sub}), thermodynamic equilibrium quality (x_e), flow quality (x), density of liquid (ρ_f) and vapor (ρ_g), specific heat of liquid ($c_{p,f}$), dynamic viscosity of liquid (μ_f), thermal conductivity of liquid (k_f), saturation temperature (T_{sat}), surface tension (σ), latent heat of vaporization (h_{fg}), molecular weight (M_w), critical pressure (p_{crit}), gravity (g), and gravitational components ($g.\sin\theta$ and $g.\cos\theta$) with respect to the channel's orientation (θ). The size of each circle represents the strength of correlation (with larger circles meaning stronger correlation), and the color represents the actual value of r.

level and channel orientation are encompassed within 3 terms. The level of gravity is explicitly provided as g/g_e, and the orientation of the channel is captured within the modified version of $1/Fr$ and Bd (originally proposed by the present authors in [12]), which capture the component of body force parallel and perpendicular to the flow, respectively. Inclusion of these 3 terms to account for body force improves the MAE of the model to 8.78%. Further additions of other parameters such as those in groups 7–9 provide no meaningful improvements.

After designating the inputs of the ANN, select model parameters, or hyperparameters of the training algorithm, including batch size, validation patience, learning rate, and network architecture, were tuned to improve the performance of the model, while other parameters listed in Table 4 are preserved. There is no definitive rule to optimize the hyperparameters and architecture of an ANN [46,52]. A manual search is employed within the ranges presented in Table 5, in which different combinations of hyperparameters are tested by trial-and-error until satisfactory performance is achieved. The finalized model including input parameters, architecture, and training parameters are listed in Table 5 and are employed for the ANNs discussed in the following section.

3. Prediction results, trends, and discussion

3.1. ANN prediction results

The trained ANN predicts the testing subset of the database with an overall MAE of 7.99%, and parity plots comparing the predictions of the ANN to the database are presented in Fig. 6. The parity plots are presented for subcooled flow boiling with single-sided heating in Fig. 6(a) and double-sided in Fig. 6(b), and saturated flow boiling with single-sided heating in Fig. 6(c) and double-sided in Fig. 6(d). The ANN predicts each subset of the test database consistently and with good accuracy. For each subset of the database, over 96% of the database is predicted within ±30% error, while over 99% is predicted within ±50% error. Furthermore, the ANN predicts 87.06% of the entire testing subset of the database within ±15% error.

3.2. Comparison of ANN to correlations

To gauge the predictive accuracy of the ANN against that of seminal correlations in the literature, a prediction assessment is performed for those correlations listed in Tables 2 and 3. The choice of seminal correlations encompasses all the general types discussed in Section 1.2.

The h correlations considered for subcooled flow boiling include Papell [67], Badiuzzaman [68], Moles and Shaw [21], Gungor and Winterton [25], Liu and Winterton [22], Shah [69], and Devahdhanush and Mudawar [11]. All correlations were developed from consolidated databases comprising different geometries, fluids, and/or wide ranges of operating conditions; see Table 2 for applicability information. The best performing correlation is one previously proposed by the present authors [11] for subcooled flow boiling of FC-72 and nPFH in rectangular channels. The database used for development was in fact consolidated from pre-launch data obtained from ground experiments at different channel orientations. After manually segregating the 2589 local datapoints into Partially Developed Boiling (PDB), Fully Developed Boiling (FDB), and Nucleate Boiling Degradation (NBD) regimes, the correlation was developed using the FDB datapoints alone. The resulting correlation yielded MAEs of 9.59, 6.91, and 41.71% for PDB, FDB, and NBD data, respectively, and an overall MAE of 20.06% [11]. It was also concluded that h for subcooled flow boiling is insignificantly affected by heating configuration and flow orientation. The present consolidated database

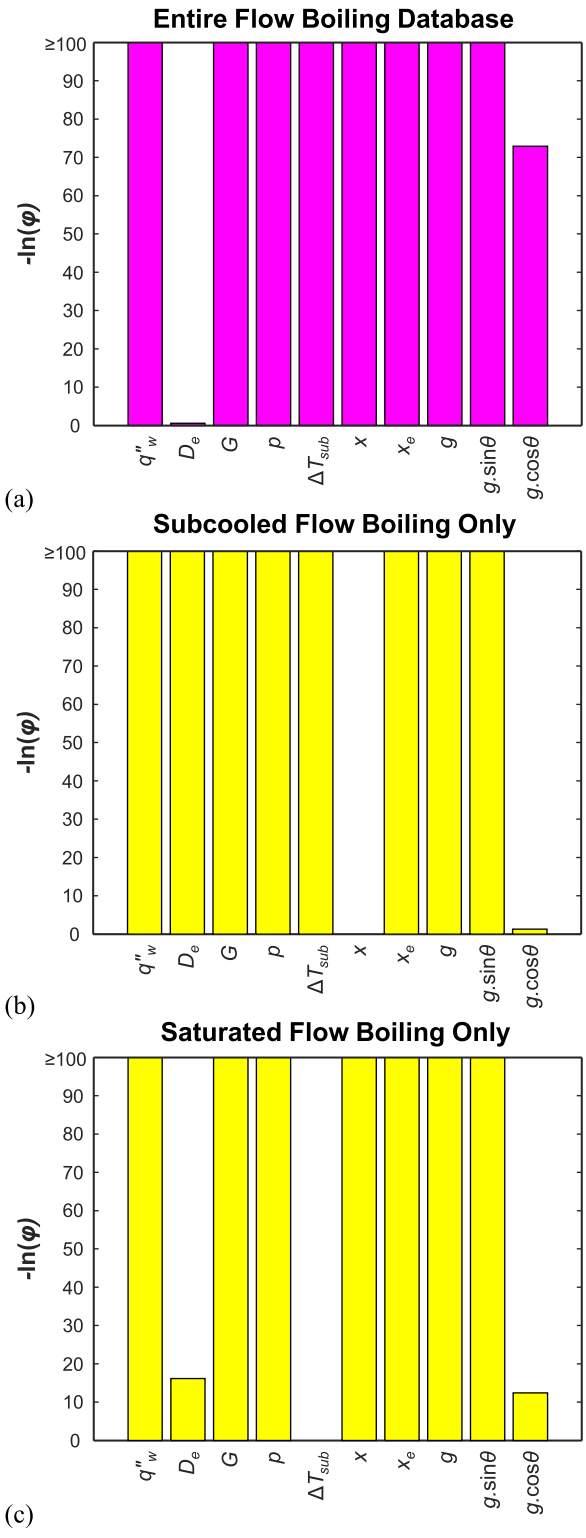

Fig. 4. F-test results of key parameters, φ, for the (a) entire database, (b) subcooled flow boiling subset of the database, and (c) saturated flow boiling subset of the database. The key parameters include wall heat flux (q''_w), equivalent heated diameter (D_e), mass velocity (G), pressure (p), degree of subcooling (ΔT_{sub}), flow quality (x), equilibrium quality (x_e), gravity (g), and gravitational components with respect to the channel's orientation (θ).

Table 4
Parameters used for training neural networks.

Parameter	Value
Max Epochs	5000
L2 Regularization	0.001
Gradient Decay Factor	0.9
Squared Gradient Decay Factor	0.999
Denominator Offset	1×10^{-8}
Learning Rate	0.001
Mini-batch Size, n	256
Validation Patience	10
Hidden Layers	5
Inputs Subcooled	$h = f(q''_w, D_e, G, p, \Delta T_{sub}, g, g.\sin\theta, g.\cos\theta)$
Inputs Saturated	$h = f(q''_w, D_e, G, p, x, g, g.\sin\theta, g.\cos\theta)$
Inputs Consolidated	$h = f(q''_w, D_e, G, p, \Delta T_{sub}, x, x_e, g, g.\sin\theta, g.\cos\theta)$

essentially contains the recently obtained ISS microgravity data in addition to the previous consolidated database, and the overall MAE with this correlation is 30.08%, meaning the correlation is reasonably applicable for subcooled flow boiling in microgravity as well. However, as already shown for the Earth gravity data in [11], the large MAE for this correlation and others stems from the substantial NBD datapoints in the consolidated database, which the correlations are generally poor at predicting. However, the newly developed ANN can predict the entire subcooled flow boiling portion of the database (including the NBD regime) with an overall MAE of ~6%, clearly outperforming all the seminal correlations assessed.

The h correlations considered for saturated flow boiling include Gungor and Winterton [25], Liu and Winterton [22], Tran et al. [70], Li and Wu [71], Kim and Mudawar [23], and Fang et al. [72]. Once again, most correlations were developed from consolidated databases comprising different geometries and fluids, and wide ranges of operating conditions; see Table 3 for applicability information. Several correlations predict at ~50% MAE, due to a considerable portion of the consolidated database belonging to the boiling regime between dryout incipience and CHF. This is due to the way the experiments were performed, with priority given to the accurate capture of CHF, requiring several fine increments of heat flux closer to CHF. Moreover, the empirical constants in these seminal correlations were determined using Earth-gravity data, leading to a questionable applicability to microgravity data. This is because saturated flow boiling is more dependent on flow orientations and body force compared to subcooled flow boiling. Saturated flow boiling is also more dependent on heating configuration due to differences in the evolution of flow regime and the associated heat transfer performance. Nevertheless, the ANN accurately predicts the saturated flow boiling datapoints independent of the boiling regime or gravitational environment. With an overall MAE of just ~9% for saturated flow boiling regime, the ANN is evidently much more accurate than the correlations assessed in this study, indicating its superiority as a prediction tool.

3.3. Assessment of the capability of ANN to predict physical trends of subcooled flow boiling in microgravity

The ANN has proved itself very accurate in predicting flow boiling heat transfer coefficients for both subcooled and saturated conditions over the entire consolidated database. However, neural network models are typically developed with a goal of predicting the entire database with the least error. ANNs are purely founded on empirical trends in the training data, and there is no flow boiling physics-based modeling done within the ANN framework. So, an assessment is required to confirm if the developed ANN can predict important parametric trends resulting from the physics of each boiling regime and environment.

To assess the trends predicted by the ANN, it is *retrained* while withholding select data from training, covering a broad range of operating conditions. These data, which are unknown to the model, are compared to the retrained ANN's predictions in select ranges of

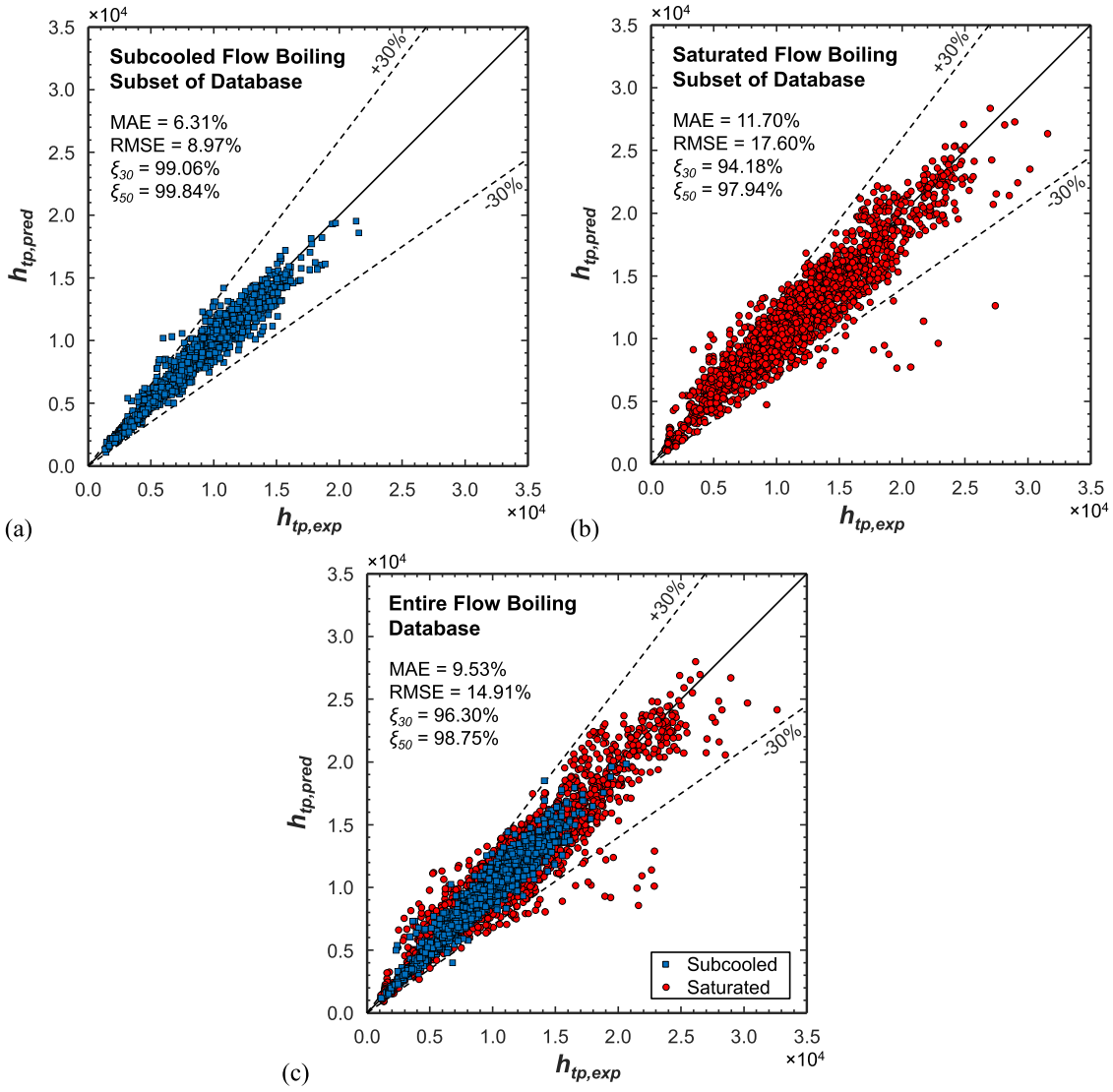

Fig. 5. Parity plots of the preliminary ANN's predictions trained for (a) the subcooled subset of the database, (b) the saturated subset of the database, and (c) the entire database. The ANN's prediction accuracy is assessed by a combination of mean absolute error (MAE), root mean square error (RMSE), and statistical inliers within ±30% (ξ_{30}) and ±50% (ξ_{50}) of experimental values.

Table 5
Ranges of parameters tested during optimization.

Parameter	Range Tested	Finalized Model
Input Parameters	$Bo, x_e, Ja^{**}, x, \ldots$	$Bo, x_e, Ja^{**}, x, \ldots$
	$\mathrm{Re}_{fo}, \mathrm{Re}_{go}, \mathrm{Re}_f, \mathrm{Re}_g, \ldots$	$\mathrm{Re}_{fo}, \mathrm{Re}_{go}, \mathrm{Re}_f, \mathrm{Re}_g, \ldots$
	$We_{fo}, We_{go}, We_f, We_g, \ldots$	$\frac{\rho_g}{\rho_f}, \frac{g}{g_e}, \frac{1}{Fr_\theta}, Bd_\theta, \frac{D_e}{D_h}$
	$p_r, \mathrm{Pr}_f, \mathrm{Pr}_g, \frac{\rho_g}{\rho_f}, \ldots$	
	$\frac{g}{g_e}, Ca, Bd, Bd_\theta, \ldots$	
	$\frac{1}{Fr_{fo}}, \frac{1}{Fr_{go}}, \frac{1}{Fr_f}, \frac{1}{Fr_g}, \frac{1}{Fr_\theta}, \ldots$	
	$La_{fo}, La_{go}, \frac{D_e}{D_h}$	
Mini-batch Size, n	16 – 512	64
Learning Rate	0.0001 – 0.01	0.001
Validation Patience	1 – 50	10
Hidden Layers	1 – 20	12

Table 6
ANN results for select groups of dimensionless inputs.

Group	Dimensionless Groups Used as Inputs to Model	MAE
1	Bo	47.46%
2	Bo, x_e, Ja^{**}, x	31.45%
3	$Bo, x_e, Ja^{**}, x, \mathrm{Re}_{fo}, \mathrm{Re}_{go}, \mathrm{Re}_f, \mathrm{Re}_g$	15.44%
4	$Bo, x_e, Ja^{**}, x, \mathrm{Re}_{fo}, \mathrm{Re}_{go}, \mathrm{Re}_f, \mathrm{Re}_g, \frac{D_e}{D_h}, \frac{\rho_g}{\rho_f}$	11.82%
5	$Bo, x_e, Ja^{**}, x, \mathrm{Re}_{fo}, \mathrm{Re}_{go}, \mathrm{Re}_f, \mathrm{Re}_g, \frac{D_e}{D_h}, \frac{\rho_g}{\rho_f}, p_r$	11.36%
6	$Bo, x_e, Ja^{**}, x, \mathrm{Re}_{fo}, \mathrm{Re}_{go}, \mathrm{Re}_f, \mathrm{Re}_g, \frac{D_e}{D_h}, \frac{\rho_g}{\rho_f}, \frac{g}{g_e}, \frac{1}{Fr_\theta}, Bd_\theta$	8.78%
7	$Bo, x_e, Ja^{**}, x, \mathrm{Re}_{fo}, \mathrm{Re}_{go}, \mathrm{Re}_f, \mathrm{Re}_g, \frac{D_e}{D_h}, \frac{\rho_g}{\rho_f}, \frac{g}{g_e}, \frac{1}{Fr_\theta}, Bd_\theta, \frac{1}{X_{tt}}$	9.11%
8	$Bo, x_e, Ja^{**}, x, \mathrm{Re}_{fo}, \mathrm{Re}_{go}, \mathrm{Re}_f, \mathrm{Re}_g, \frac{D_e}{D_h}, \frac{\rho_g}{\rho_f}, \frac{g}{g_e}, \frac{1}{Fr_\theta}, Bd_\theta, La_{fo}, La_{go}$	8.94%
9	$Bo, x_e, Ja^{**}, x, \mathrm{Re}_{fo}, \mathrm{Re}_{go}, \mathrm{Re}_f, \mathrm{Re}_g, \frac{D_e}{D_h}, \frac{\rho_g}{\rho_f}, \frac{g}{g_e}, \frac{1}{Fr_\theta}, Bd_\theta, We_{fo}, We_{go}, We_f, We_g$	9.31%

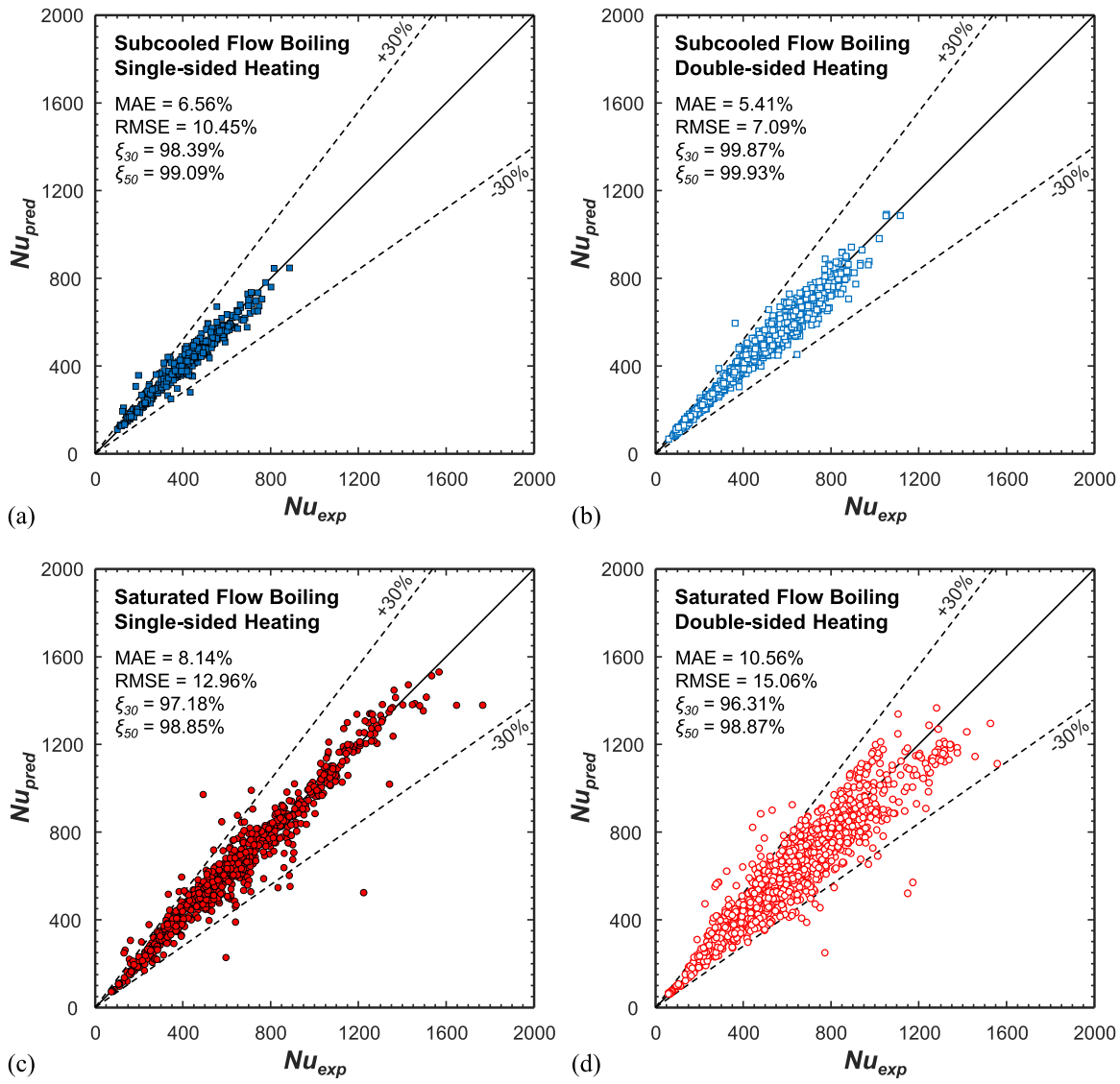

Fig. 6. Parity plots of the final ANN's predictions for subcooled flow boiling with (a) single- and (b) double-sided heating and saturated flow boiling with (c) single- and (d) double-sided heating. The ANN's prediction accuracy is assessed by a combination of mean absolute error (MAE), root mean square error (RMSE), and statistical inliers within ±30% (ξ_{30}) and ±50% (ξ_{50}) of experimental values.

operating parameters. Fig. 7 compares Nu_{tp} trends predicted by the ANN with data excluded from training for single-sided heating in μg_e and focusing on subcooled conditions (with some protuberance into saturated). Each subfigure plots Nu_{tp} with respect to x_e at different q''_w for a given range of G and p. Figs. 7(a-c) feature predictions for highly subcooled conditions at $G \approx$ 200, 800, and 2400 kg/m^{2}s, respectively. At each G, the ANN captures relatively constant Nu_{tp} with respect to x_e, but increasing Nu_{tp} upon increasing q''_w. A similar trend is observed for fixed q''_w, where increasing G yields nearly constant Nu_{tp}, as shown at $q''_w \approx$ 20 W/cm^2, resulting in $Nu_{tp} \approx$ 300 at each G. These trends are traits of nucleate boiling dominance, which is expected during highly subcooled flow boiling. Figs. 7(d-f) respectively depict, for $G \approx$ 200, 800, and 2400 kg/m^{2}s, a much higher x_e, which even transitions to saturated flow boiling in some cases. At low G, Fig. 7(d), Nu_{tp} is predicted to increase with increasing x_e for $q''_w =$ 5.34 W/cm^2 but decrease for $q''_w =$ 9.72 W/cm^2 as the flow becomes saturated, capturing the physics of degradation of nucleate boiling at relatively high q''_w. However, at $G \approx$ 800 kg/m^{2}s, Fig. 7(e), Nu_{tp} is predicted to increase with increasing x_e, even at $q''_w =$ 19.55 W/cm^2, and predictions overlap for different q''_w due to the growing influence of convective boiling. At $G \approx$ 2400 kg/m^{2}s, Fig. 7(f), predictions of Nu_{tp} are greater for $q''_w =$ 24.69 than 33.67 W/cm^2, and different trends are captured. At the lower q''_w, the ANN predicts Nu_{tp} increasing with increasing x_e as the flow approaches saturation but relatively constant Nu_{tp} at high q''_w, capturing the degradation of nucleate boiling offsetting the enhancement of Nu_{tp} as the fluid becomes saturated.

Fig. 8 depicts similar plots as Fig. 7 but for double-sided heating. During double-sided heating, a broader range of x_e is captured compared to single-sided, due to heat addition from two walls. Fig. 8(a) shows ANN predictions for $G \approx$ 200 kg/m^{2}s with high subcooling. At $q''_w =$ 9.64 W/cm^2, the range of x_e is relatively small and Nu_{tp} marginally increases with x_e. However, at higher q''_w, the range of x_e increases, and the increase in Nu_{tp} is greater. As the fluid approaches saturation, Nu_{tp} predictions for $q''_w =$ 14.50 and 19.77 W/cm^2 converge. At higher G, Figs. 8(b) and 8(c), the span of x_e is lesser than in Fig. 8(a), and the ANN predicts a relatively constant Nu_{tp}. Fig. 8(d) shows predicted trends for $G \approx$ 200 kg/m^{2}s with low subcooling and transitioning to saturated. At low q''_w of 5.07 and 9.64 W/cm^2, the ANN captures the increase in Nu_{tp} as the flow becomes saturated. At $q''_w =$ 17.02 W/cm^2, the fluid is mostly saturated, and the ANN predicts the degradation of Nu_{tp} as x_e increases for high q''_w and low G. Fig. 8(e) presents predicted trends for $G \approx$ 800 kg/m^{2}s. The ANN predicts Nu_{tp} to be the largest for the intermediate q''_w

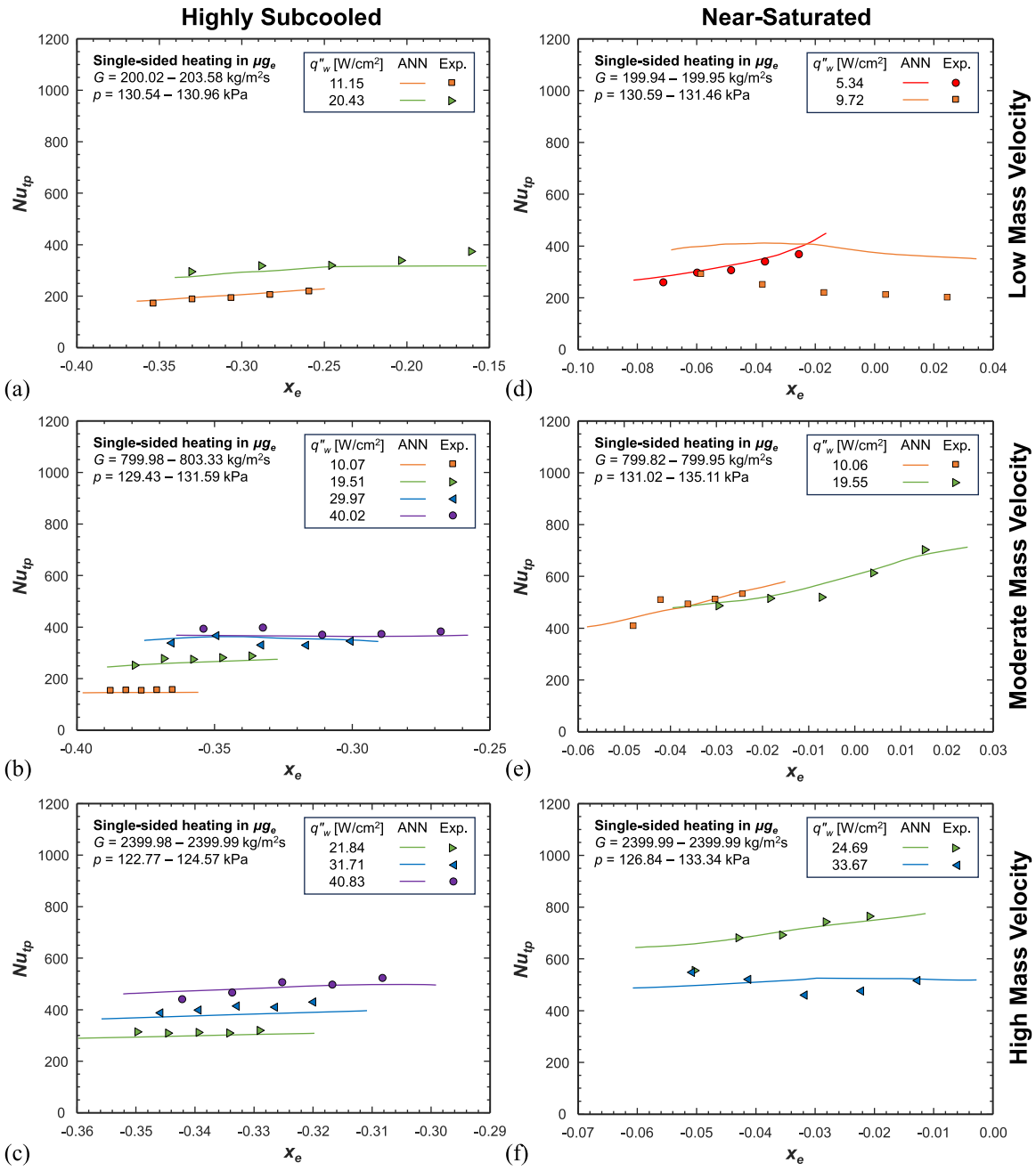

Fig. 7. Parametric trends of two-phase Nusselt number, Nu_{tp}, with respect to equilibrium quality, x_e, predicted by the ANN compared to corresponding experimental data excluded from training. Each plot shows predictions for single-sided heating at different heat fluxes, q''_w, for high subcooling at mass velocities of $G \approx$ (a) 200, (b) 800, and (c) 2400 kg/m^{2}s and near-saturation at mass velocities of $G \approx$ (d) 200, (e) 800, and (f) 2400 kg/m^{2}s.

of 20.16 W/cm^2 and captures trends of Nu_{tp} near the transition to saturated flow boiling. At $G \approx 2400$ kg/m^{2}s, Fig. 8(f), the ANN captures greater Nu_{tp} at $q''_w = 32.20$ than 23.06 W/cm^2 but appears to overpredict the slope of Nu_{tp} with respect to x_e as saturation is approached. The ANN compensates for the first point at each q''_w that is significantly lower than those closer to saturation, which are nearly constant, resulting in a trend where the ANN predicts a steady increase in Nu_{tp} as saturation is approached. Overall, the ANN still predicts Nu_{tp} reasonably well in this range.

3.4. Assessment of the capability of ANN to predict physical trends of saturated flow boiling in microgravity

Fig. 9 plots ANN predictions of Nu_{tp} in μg_e for saturated flow boiling with single-sided heating. Figs. 9(a) and 9(b) include cases with relatively low x_e and $G \approx 180$ and 2400 kg/m^{2}s, respectively. At both G, the ANN captures the degradation of Nu_{tp} as q''_w increases. However, upon increasing x_e, Nu_{tp} is constant at low G but increases at high G due to stronger convective effects. Predictions for a higher range of x_e are shown in Figs. 9(c) and 9(d) for $G \approx 380$ and 790 kg/m^{2}s. At high x_e, the ANN captures decreasing Nu_{tp} with increasing q''_w, similar to low x_e, and diminishing Nu_{tp} as x_e is further increased.

Fig. 10 compares the predictions of the ANN for saturated flow boiling in μg_e with double-sided heating to the corresponding data excluded from training. At low x_e and $G \approx 180$ kg/m^{2}s, the ANN predicts nearly identical Nu_{tp} at $q''_w = 5.32$ than 10.36 W/cm^2, but different trends are observed. Nu_{tp} increases upon increasing x_e at $q''_w = 5.32$ W/cm^2 but decreases upon increasing x_e at $q''_w = 10.36$ W/cm^2, capturing

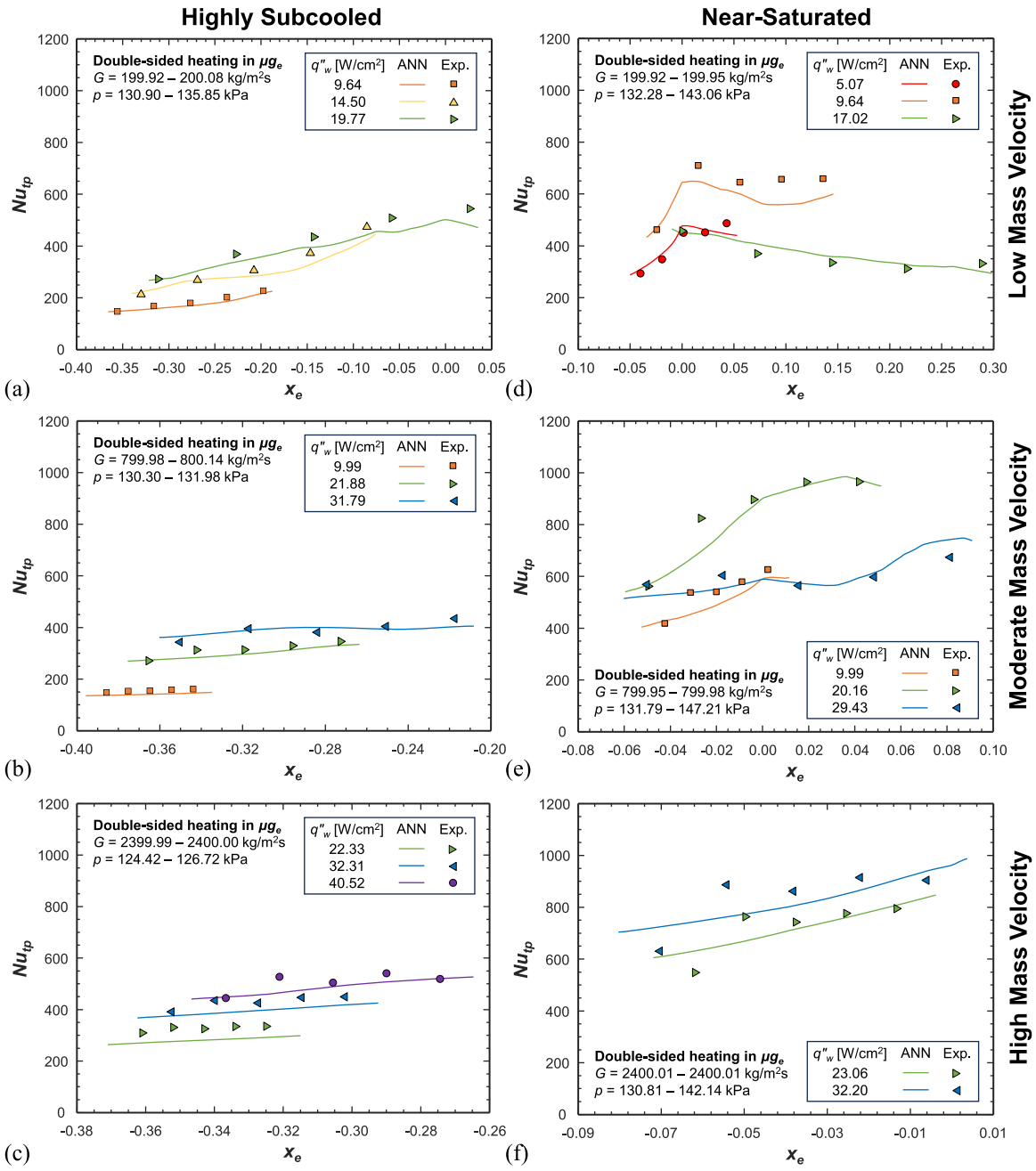

Fig. 8. Parametric trends of two-phase Nusselt number, Nu_{tp}, with respect to equilibrium quality, x_e, predicted by the ANN compared to corresponding experimental data excluded from training. Each plot shows predictions for double-sided heating at different heat fluxes, q''_w, for high subcooling at mass velocities of $G \approx$ (a) 200, (b) 800, and (c) 2400 kg/m^{2}s and near-saturation at mass velocities of $G \approx$ (d) 200, (e) 800, and (f) 2400 kg/m^{2}s.

the enhancement of convective boiling and the degradation of nucleate boiling, respectively. At $G \approx 2400$ kg/m^{2}s, shown in Fig. 10(b), similar Nu_{tp} is predicted at both $q''_w = 23.89$ and 33.66 W/cm^2. However, similar to Figs. 8(f) and 9(b) the ANN smoothens the abrupt increase in Nu_{tp} that occurs near the transition to saturated flow boiling at $q''_w = 23.89$ W/cm^2. At the highest q''_w of 37.97 W/cm^2, the ANN accurately predicts Nu_{tp} and captures the diminishment of Nu_{tp} as x_e increases. In Fig. 10(c) and 10(d), featuring high x_e and $G \approx 380$ and 790 kg/m^{2}s, respectively, the ANN predicts a relatively constant Nu_{tp} at the lower q''_w, but the experimental trend shows a slight decrease in Nu_{tp}. However, at higher q''_w, the degradation of Nu_{tp} with increasing x_e is more apparent and the trend is accurately captured by the ANN.

3.5. *Assessment of the capability of ANN to predict physical trends of flow boiling in different body force environments*

The ANN has displayed proficiency in predicting Nu_{tp} during flow boiling at a wide variety of conditions in μg_e. But its performance in predicting the physical trends of flow boiling in different body force environments is still uncertain; this aspect is assessed here.

Fig. 11 shows trends captured by the ANN in μg_e compared to those predicted for flow boiling in g_e at different orientations. Figs. 11(a) and 11(b) focus on single-sided heating during high-quality saturated flow boiling and double-sided heating during low-quality subcooled flow boiling, respectively. In Fig. 11(a), the ANN predicts a relatively constant Nu_{tp} with respect to x_e at each orientation, while the experimental data show some variation. Regardless, Nu_{tp} is predicted with good

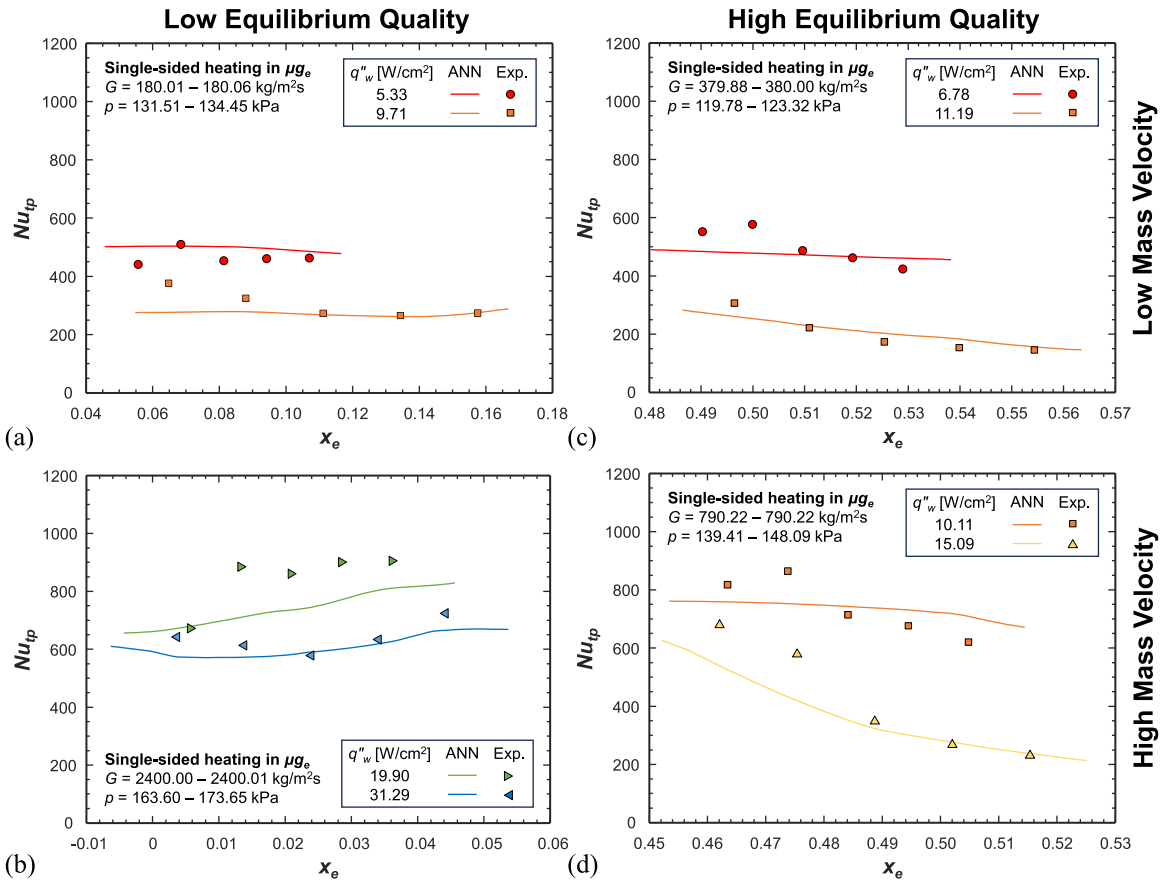

Fig. 9. Parametric trends of two-phase Nusselt number, Nu_{tp}, with respect to equilibrium quality, x_e, predicted by the ANN compared to corresponding experimental data excluded from training. Each plot shows predictions for single-sided heating at different heat fluxes, q''_w, for relatively low x_e at mass velocities of $G \approx$ (a) 180 and (b) 2400 kg/m²s and relatively high x_e at mass velocities of $G \approx$ (c) 380 and (d) 790 kg/m²s.

accuracy at each orientation. In Fig. 11(b), both the trend and value of Nu_{tp} is predicted well by the ANN, and the predicted Nu_{tp} is similar at different orientations due to the dominance of nucleate boiling at high subcooling.

3.6. Application of ANNs to other fluids and heating configurations

The present ANN is developed and trained using the FBCE consolidated heat transfer database which features flow boiling data for a single fluid, nPFH, in a partially heated rectangular channel with 1 or 2 opposite heated walls. The present database highlights the gravitational effects on flow boiling, which is of particular interest to nPFH due to its for potential as the working fluid for thermal management systems in aerospace applications [77]. However, it is of interest to explore the predictive capability of the developed ANN to other unique databases. The trained ANN is used to predict the database of Cioncolini et al. [78], which contains 133 data points of water flow boiling in a uniformly heated tube. The same ANN that predicted the consolidated FBCE heat transfer database with an MAE of 7.99% is incapable of predicting the Nu_{tp} for the water database of Cioncolini et al. [78] evidenced by a comparatively high MAE. However, if the developed ANN is again *retrained*, but including the water data prior to dividing the database into the *training*, *testing*, and *validation* subsets, the water data in the testing subset is predicted with an MAE of 13.04%. The massive improvement in MAE for the water data was compensated for with a small decrease in the accuracy of the nPFH predictions, which was still predicted with an MAE of 8.29%. While the scope of the FBCE database limits the accuracy of the model when extrapolated to other fluids or channel geometries, the methods used to develop the ANN in this study can be applied to other databases to achieve high accuracy predictions for other fluids and heating configurations.

4. Artificial neural network for critical heat flux

4.1. Consolidated database, model development, ANN's predictive performance, and comparison to correlations

Because of the success of the ANN developed for heat transfer coefficient, an ANN is developed to predict flow boiling CHF for a consolidated FBCE CHF database, presented in Table 7.

In a previous study by the present authors [12], an exhaustive literature review and correlation assessment was performed with the consolidated database prior to the addition of the microgravity data obtained onboard the ISS. The authors assessed the importance of various dimensionless groups and proposed the following correlation,

$$Bo_{CHF} = 0.353 We_{D_e}^{-0.314} \left(\frac{L_h}{D_e}\right)^{-0.226} \left(\frac{\rho_f}{\rho_g}\right)^{-0.481} \cdots \left(1 - \left(\frac{\rho_f}{\rho_g}\right)^{-0.094} x_{e,in}\right) \left(1 + 0.034 \frac{1}{Fr_{\theta,D_e}}\right) \cdots \left(1 + 0.008 \frac{Bd_{\theta,D_e}}{We_{D_e}^{0.543}}\right). \quad (25)$$

The correlation proved its robustness with an overall MAE of 17.44% for the prelaunch database, outperforming all other correlations tested. The correlation later showed its superiority over others in predicting q''_{CHF} in μg_e for data obtained onboard the ISS with subcooled inlet having 18.5% MAE [16] and saturated two-phase inlet having 22.4%

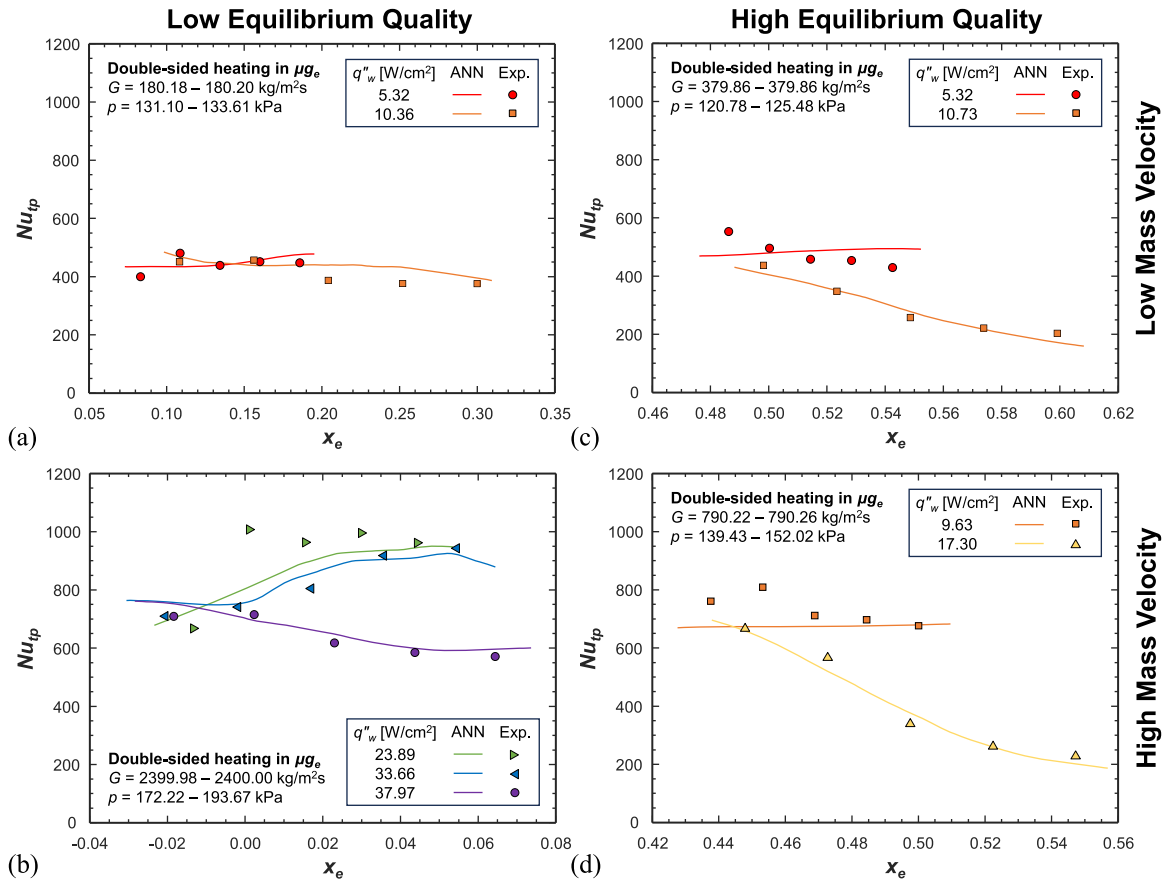

Fig. 10. Parametric trends of two-phase Nusselt number, Nu_{tp}, with respect to equilibrium quality, x_e, predicted by the ANN compared to corresponding experimental data excluded from training. Each plot shows predictions for double-sided heating at different heat fluxes, q''_w, for relatively low x_e at mass velocities of $G \approx$ (a) 180 and (b) 2400 kg/m^{2}s and relatively high x_e at mass velocities of $G \approx$ (c) 380 and (d) 790 kg/m^{2}s.

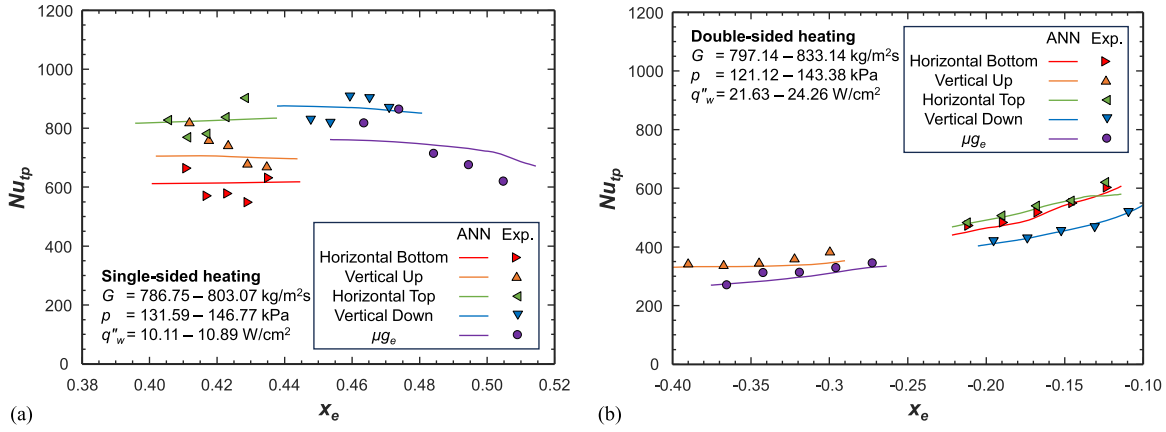

Fig. 11. Parametric trends of two-phase Nusselt number, Nu_{tp}, with respect to equilibrium quality, x_e, predicted by the ANN compared to corresponding experimental data excluded from training. Each plot shows trends predicted in μg_e and different orientations in g_e for (a) single-sided heating at mass velocity of $G \approx$ 800 kg/m^{2}s, heat flux of $q''_w \approx$ 10 W/cm^2, and high x_e, and (b) double-sided heating at $G \approx$ 800 kg/m^{2}s, $q''_w \approx$ 23 W/cm^2, and low x_e.

MAE [17]. The entire consolidated FBCE CHF database is predicted with an MAE of 18.07%. Hence, the dimensionless groups included in Eq. (25) are employed as input parameters for the ANN to predict Bo_{CHF} developed in this section.

The overall methodology of setting up the ANN for CHF and optimization using the manual search method is identical to that described for heat transfer in Section 2.3.2. Table 8 shows the final selected parameters to train the model, with other parameters identical to Table 4. A parity plot of the testing data for the final ANN is shown in Fig. 12. Even with the relatively small size of the CHF database, the trained model is accurate in predicting the testing data with a 12.05% MAE.

The ANN clearly outperforms the correlation in Eq. (25), which predicted the testing subset of the database with a 23.41% MAE and has previously shown its superiority to other correlations for the present database [12,16,17].

Table 7
Summary of consolidated FBCE-CHF database.

Heating Configuration	Single-sided					Double-sided				Overall
Flow Orientation/ Environment	Horizontal Bottom	Horizontal Top	Vertical Up	Vertical Down	μg_e	Horizontal	Vertical Up	Vertical Down	μg_e	
N	54	53	55	32	108	74	72	47	146	641
G [kg/m^{2}s]	99.09 – 3199.28	194.89 – 3200.9	179.70 – 3199.97	199.34 – 2030.27	179.99 – 3199.98	144.24 – 3211.55	175.30 – 3199.96	200.97 – 2314.43	179.90 – 3199.97	99.09 – 3211.55
p_{in} [kPa]	98.41 – 184.26	97.12 – 180.72	110.33 – 181.75	119.38 – 182.29	117.19 – 178.84	97.10 – 221.04	109.71 – 229.77	107.20 – 239.48	109.77 – 200.44	97.10 – 239.48
T_{in} [°C]	23.35 – 76.87	28.55 – 77.29	34.32 – 79.10	58.88 – 80.60	23.55 – 77.84	23.15 – 78.75	26.12 – 80.00	27.93 – 81.30	25.51 – 80.69	23.15 – 81.30
$\Delta T_{sub,in}$ [°C]	0.00 – 28.31	0.00 – 31.17	0.00 – 31.65	0.00	0.00 – 45.59	0.00 – 35.63	0.00 – 36.67	0.00 – 37.54	0.00 – 43.71	0.00 – 45.59
$x_{e,in}$	-0.362 – 0.633	-0.401 – 0.658	-0.420 – -0.686	0.000 – 0.668	-0.609 – 0.863	-0.455 – 0.635	-0.477 – 0.678	-0.495 – 0.656	-0.585 – 0.862	-0.609 – 0.863
p_{out} [kPa]	96.70 – 159.11	95.68 – 158.13	108.02 – 167.90	114.83 – 154.38	112.88 – 167.37	96.51 – 215.65	106.93 – 223.68	107.81 – 234.23	108.07 – 181.19	95.68 – 234.23
T_{out} [°C]	34.52 – 67.74	31.88 – 67.48	39.94 – 71.41	53.66 – 66.52	34.82 – 70.61	37.45 – 78.27	40.83 – 79.62	37.84 – 79.00	43.06 – 79.08	31.88 – 79.62
$\Delta T_{sub,out}$ [°C]	0.00 – 23.07	0.00 – 25.22	0.00 – 20.51	0.00	0.00 – 34.50	0.00 – 23.49	0.00 – 29.01	0.00 – 27.93	0.00 – 20.55	0.00 – 34.50
$x_{e,out}$	-0.308 – 0.779	-0.302 – 0.720	-0.269 – 0.794	0.027 – 0.766	-0.452 – 0.936	-0.391 – 0.781	-0.495 – 0.901	-0.420 – 0.866	-0.256 – 0.974	-0.495 – 0.974
q''_{CHF} [W/cm^2]	11.31 – 42.31	3.77 – 42.89	8.38 – 50.62	6.48 – 23.09	7.87 – 53.91	4.05 – 50.81	8.82 – 50.57	6.15 – 23.42	6.12 – 48.88	3.77 – 53.91

Table 8
Final selected parameters for the ANN for CHF.

Parameter	Finalized Model
Input Parameters	$We_{De}, \frac{L_h}{D_e}, \frac{\rho_f}{\rho_g}, x_{e,in}, \frac{1}{Fr_{\theta,De}}, Bd_{\theta,De}$
Mini-batch Size	16
Learning Rate	0.0001
Validation Patience	30
Hidden Layers	13

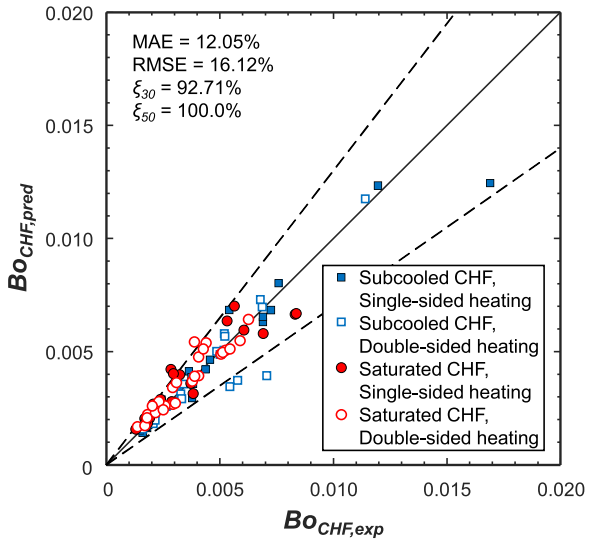

Fig. 12. Parity plot comparing the predictions of the ANN trained for CHF to the testing subset of the consolidated FBCE CHF database. The prediction accuracy of the CHF ANN is assessed by a combination of mean absolute error (MAE), root mean square error (RMSE), and statistical inliers within ±30% (ξ_{30}) and ±50% (ξ_{50}) of experimental values.

4.2. Assessment of the capability of ANN to predict physical trends of CHF in microgravity

Once again, the capability of the ANN in predicting physical trends is assessed for CHF. Fig. 13 depicts parametric trends predicted by the ANN for data within the testing subset of the CHF database. Fig. 13(a) shows predictions for single-sided heating with the inlet condition ranging from subcooled to low-quality saturated. Generally, as $x_{e,in}$ increases, Bo_{CHF} is predicted to decrease, level off, and even slightly increase as inlet conditions transition to saturated. Overall, the ANN predicts the transition to saturated inlet reasonably well. Moreover, it accurately captures the expected trend of Bo_{CHF} deteriorating upon increasing G. Fig. 13(b) shows predictions for ranges within the testing subset of the database with double-sided heating, which comprises broader ranges of $x_{e,in}$. At highly subcooled conditions, *i.e.*, low $x_{e,in}$, the ANN captures decreasing Bo_{CHF} with increasing $x_{e,in}$. The ANN predicts Bo_{CHF} to be relatively constant near saturation, and it to decrease at high $x_{e,in}$, confirming the ANN's capability to capture various physical trends within the database.

5. Conclusions

This study, a part of the Flow Boiling and Condensation Experiment (FBCE), had the goal of developing a prediction tool for heat transfer and CHF for flow boiling in both microgravity and Earth gravity based on artificial neural networks (ANN). The experimental database, used for developing/training the ANN, was made by consolidating data from experiments onboard the International Space Station (ISS) and at different orientations on Earth. A summary of this study is provided below:

(1) The consolidated FBCE heat transfer coefficient database comprised 29,226 datapoints spanning a wide range of operating conditions for nPFH or FC-72 flow boiling in a rectangular channel heated along one or two walls. The ranges of parameters include mass velocity of 173 – 3200 kg/m^{2}s, pressure of 102 – 238 kPa, subcooling of 0 – 44°C, and thermodynamic equilibrium quality of -0.60 – 0.95 (spanning all the way from highly subcooled to high-quality saturated boiling). The resulting heat transfer coefficients ranged from 1070 to 32,649 W/m^{2}K. The entire database is randomly divided into training data (70%), testing data (15%) and validation data (15%).
(2) Following a meticulous statistical analysis of various input parameters relevant to flow boiling and optimization of key model parameters and options, a fully connected feed-forward ANN was

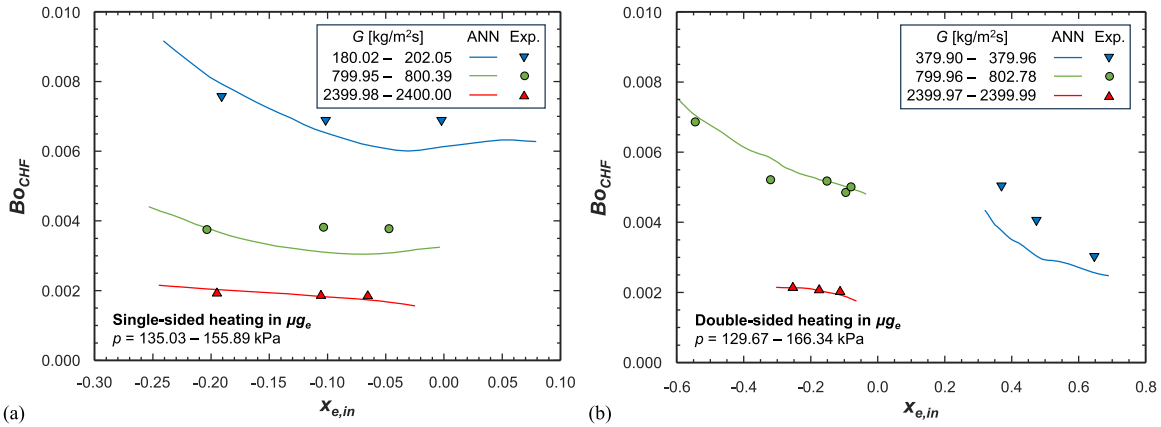

Fig. 13. Parametric trends of Boiling number at CHF, Bo_{CHF}, with respect to inlet equilibrium quality, $x_{e,in}$, predicted by the CHF ANN compared to corresponding data in the testing subset of the experimental database. Each plot shows trends predicted in μg_e at different mass velocities, G, for (a) single- and (b) double-sided heating.

developed to predict flow boiling heat transfer. The final ANN relies upon dimensionless inputs relative to flow boiling, consists of 12 hidden layers, and is trained using Adam to predict Nu_{tp}. The final ANN predicts the entire test database with an overall MAE of just 7.99%, with consistent and high accuracy predictions of each subset (subcooled or saturated flow boiling with single- or double-sided heating). For each subset, over 96% of the testing database is predicted within ± 30% error, while over 99% is predicted within ±50% error. The ANN outperformed existing seminal correlations for both subcooled and saturated flow boiling, proving its superiority. Moreover, the model proved its robustness by accurately predicting physical parametric trends in previously unseen data, including constant independence of Nu_{tp} on x_e during nucleate boiling dominant subcooled boiling, enhanced heat transfer with increasing G, and the transition from subcooled to saturated flow boiling.

(3) Similar to heat transfer, the CHF datapoints from FBCE were consolidated into a database of 641 points spanning mass velocity of 99 – 3212 kg/m^{2}s, inlet pressure of 97 – 239 kPa, inlet subcooling of 0 – 46°C, inlet thermodynamic equilibrium quality of -0.61 – 0.86, and CHF values of 4 – 54 W/cm^2.

(4) A separate ANN was developed and trained to predict flow boiling CHF. The overall methodology of this ANN was maintained identical to the heat transfer ANN. The final model consists of 13 hidden layers and is optimized to predict dimensionless CHF, Bo_{CHF}. The CHF ANN was very accurate in predicting the testing data with an overall MAE of just 12.05%. This is far better than the most accurate CHF correlation, which was incidentally one by the present authors and predicts the consolidated FBCE CHF database with an MAE of 18.07%.

(5) The artificial neural networks' high prediction accuracy, in conjunction with their ability to predict parametric physical trends, shows their evident superior capability of serving as prediction tools for both heat transfer and CHF for flow boiling in microgravity and Earth gravity.

Data availability

The experimental raw data used in this paper will be publicly made available in a NASA repository later.

CRediT authorship contribution statement

Issam Mudawar: Conceptualization, Methodology, Supervision, Writing – review & editing, Funding acquisition. **Steven J. Darges:** Validation, Software, Formal analysis, Investigation, Writing – original draft. **V.S. Devahdhanush:** Methodology, Formal analysis, Investigation, Data curation, Writing – original draft, Writing – review & editing.

Declaration of Competing Interest

The authors declare that they have no known competing financial interests or personal relationships that could have appeared to influence the work reported in this paper.

Acknowledgments

The authors acknowledge the support of the National Aeronautics and Space Administration (NASA) under grant no. 80NSSC22K0328. The authors thank their collaborators at NASA Glenn Research Center, especially Mohammad M. Hasan, Henry K. Nahra, R. Balasubramaniam, and Jeffrey R. Mackey. The authors also thank the FBCE team at NASA Glenn Research Center, Cleveland, Ohio, especially Nancy Hall (FBCE Project Manager), Rochelle May and Phillip Gonia (Software Engineering), Mark Sorrells (Assembly, Integration and Test Lead), Jesse DeFiebre (Fluids Lead), Monica Guzik (FBCE Chief Engineer), and ZIN FCF Mission Operations Team, for their dedicated technical assistance and successful completion of ISS testing of FBCE's FBM.

References

[1] F.P. Chiaramonte, J. McQuillen, H.K. Nahra, P. Manoharan, H. Vanhala, B.J. Motil, J. Kim, V. Carey, W.G. Anderson, J. Plawsky, L. Carter, A. Jackson, 2019 NASA division of space and life and phyiscal sciences research and applications fluid physics workshop report, Cleveland, OH, USA, 2020.

[2] C. Konishi, I. Mudawar, Review of flow boiling and critical heat flux in microgravity, Int. J. Heat Mass Transf. 80 (2015) 469–493, https://doi.org/10.1016/j.ijheatmasstransfer.2014.09.017.

[3] R. Raj, J. Kim, J. McQuillen, Pool boiling heat transfer on the international space station: Experimental results and model verification, J. Heat Transf. 134 (10) (2012), 101504, https://doi.org/10.1115/1.4006846.

[4] V.K. Dhir, G.R. Warrier, E. Aktinol, D. Chao, J. Eggers, W. Sheredy, W. Booth, Nucleate pool boiling experiments (NPBX) on the international space station, Microgravity Sci. Technol. 24 (5) (2012) 307–325, https://doi.org/10.1007/s12217-012-9315-8.

[5] K. Inoue, H. Ohta, Y. Toyoshima, H. Asano, O. Kawanami, R. Imai, K. Suzuki, Y. Shinmoto, S. Matsumoto, Heat loss analysis of flow boiling experiments onboard international space station with unclear thermal environmental conditions (1st report: subcooled liquid flow conditions at test section inlet), Microgravity Sci. Tec. 33 (2) (2021) 28, https://doi.org/10.1007/s12217-021-09869-5.

[6] A. Sielaff, D. Mangini, O. Kabov, M.Q. Raza, A.I. Garivalis, M. Zupančič, S. Dehaeck, S. Evgenidis, C. Jacobs, D. Van Hoof, O. Oikonomidou, X. Zabulis, P. Karamaounas, A. Bender, F. Ronshin, M. Schinnerl, J. Sebilleau, C. Colin, P. Di Marco, T. Karapantsios, I. Golobič, A. Rednikov, P. Colinet, P. Stephan, L. Tadrist, The multiscale boiling investigation on-board the International Space Station: An overview, Appl. Therm. Eng. 205 (2022), 117932, https://doi.org/10.1016/j.applthermaleng.2021.117932.

[7] P. Chorin, A. Boned, J. Sebilleau, C. Colin, O. Schoele-Schulz, N. Picchi, C. Schwarz, B. Toth, D. Mangini, Conception of a compact flow boiling loop for the international space station- first results in parabolic flights, C. R. Méc. 351 (S2) (2023) 1–20, https://doi.org/10.5802/crmeca.147.

[8] H. Zhang, I. Mudawar, M.M. Hasan, Experimental and theoretical study of orientation effects on flow boiling CHF, Int. J. Heat Mass Transf. 45 (22) (2002) 4463–4477, https://doi.org/10.1016/S0017-9310(02)00152-7.

[9] C. Konishi, H. Lee, I. Mudawar, M.M. Hasan, H.K. Nahra, N.R. Hall, J.D. Wagner, R. L. May, J.R. Mackey, Flow boiling in microgravity: Part 2 - critical heat flux interfacial behavior, experimental data, and model, Int. J. Heat Mass Transf. 81 (2015) 721–736, https://doi.org/10.1016/j.ijheatmasstransfer.2014.10.052.

[10] V.S. Devahdhanush, I. Mudawar, H.K. Nahra, R. Balasubramaniam, M.M. Hasan, J. R. Mackey, Experimental heat transfer results and flow visualization of vertical upflow boiling in Earth gravity with subcooled inlet conditions–in preparation for experiments onboard the international space station, Int. J. Heat Mass Transf. 188 (2022), 122603, https://doi.org/10.1016/j.ijheatmasstransfer.2022.122603.

[11] V.S. Devahdhanush, I. Mudawar, Subcooled flow boiling heat transfer in a partially-heated rectangular channel at different orientations in Earth gravity, Int. J. Heat Mass Transf. 195 (2022), 123200, https://doi.org/10.1016/j.ijheatmasstransfer.2022.123200.

[12] S.J. Darges, V.S. Devahdhanush, I. Mudawar, Assessment and development of flow boiling critical heat flux correlations for partially heated rectangular channels in different gravitational environments, Int. J. Heat Mass Transf. 196 (2022), 123291, https://doi.org/10.1016/j.ijheatmasstransfer.2022.123291.

[13] I. Mudawar, V.S. Devahdhanush, S.J. Darges, M.M. Hasan, H.K. Nahra, R. Balasubramaniam, J.R. Mackey, Heat transfer and interfacial flow physics of microgravity flow boiling in single-side-heated rectangular channel with subcooled inlet conditions–experiments onboard the international space station, Int. J. Heat Mass Transf. 207 (2023), 123998, https://doi.org/10.1016/j.ijheatmasstransfer.2023.123998.

[14] I. Mudawar, V.S. Devahdhanush, S.J. Darges, M.M. Hasan, H.K. Nahra, R. Balasubramaniam, J.R. Mackey, Effects of heating configuration and operating parameters on heat transfer and interfacial physics of microgravity flow boiling with subcooled inlet conditions–experiments onboard the international space station, Int. J. Heat Mass Transf. 217 (2023), 124732, https://doi.org/10.1016/j.ijheatmasstransfer.2023.124732.

[15] I. Mudawar, V.S. Devahdhanush, S.J. Darges, M.M. Hasan, H.K. Nahra, R. Balasubramaniam, J.R. Mackey, Microgravity flow boiling experiments with liquid-vapor mixture inlet onboard the international space station, Int. J. Heat Mass Transf. (2023) under review.

[16] I. Mudawar, S.J. Darges, V.S. Devahdhanush, Parametric experimental trends, interfacial behavior, correlation assessment, and interfacial lift-off model predictions of critical heat flux for microgravity flow boiling with subcooled inlet conditions–experiments onboard the international space station, Int. J. Heat Mass Transf. 213 (2023), 124296, https://doi.org/10.1016/j.ijheatmasstransfer.2023.124296.

[17] I. Mudawar, S.J. Darges, V.S. Devahdhanush, Critical heat flux for microgravity flow boiling with two-phase inlet conditions - experiments onboard the international space station, Int. J. Heat Mass Transf. (2023) under review.

[18] X. Fang, Y. Yuan, A. Xu, L. Tian, Q. Wu, Review of correlations for subcooled flow boiling heat transfer and assessment of their applicability to water, Fusion Eng. Des. 122 (2017) 52–63, https://doi.org/10.1016/j.fusengdes.2017.09.008.

[19] X. Fang, F. Zhuang, C. Chen, Q. Wu, Y. Chen, Y. Chen, Y. He, Saturated flow boiling heat transfer: review and assessment of prediction methods, Heat Mass Transf. 55 (1) (2019) 197–222, https://doi.org/10.1007/s00231-018-2432-1.

[20] D.B.R. Kenning, M.G. Cooper, Saturated flow boiling of water in vertical tubes, Int. J. Heat Mass Transf. 32 (3) (1989) 445–458, https://doi.org/10.1016/0017-9310(89)90132-4.

[21] F.D. Moles, J.F.G. Shaw, Boiling heat-transfer to sub-cooled liquids under conditions of forced convection, Trans. Inst. Chem. Eng. Chem. Eng. 50 (1) (1972) 76–84.

[22] Z. Liu, R.H.S. Winterton, A general correlation for saturated and subcooled flow boiling in tubes and annuli, based on a nucleate pool boiling equation, Int. J. Heat Mass Transf. 34 (11) (1991) 2759–2766, https://doi.org/10.1016/0017-9310(91)90234-6.

[23] S.M. Kim, I. Mudawar, Universal approach to predicting saturated flow boiling heat transfer in mini/micro-channels–part ii. two-phase heat transfer coefficient, Int. J. Heat Mass Transf. 64 (2013) 1239–1256, https://doi.org/10.1016/j.ijheatmasstransfer.2013.04.014.

[24] J.C. Chen, Correlation for boiling heat transfer to saturated fluids in convective flow, Ind. Eng. Chem. Process Des. Dev. 5 (3) (1966) 322–329, https://doi.org/10.1021/i260019a023.

[25] K.E. Gungor, R.H.S. Winterton, A general correlation for flow boiling in tubes and annuli, Int. J. Heat Mass Transf. 29 (3) (1986) 351–358, https://doi.org/10.1016/0017-9310(86)90205-X.

[26] K. Il Choi, A.S. Pamitran, J.T. Oh, Two-phase flow heat transfer of CO2 vaporization in smooth horizontal minichannels, Int. J. Refrig. 30 (5) (2007) 767–777, https://doi.org/10.1016/j.ijrefrig.2006.12.006.

[27] S.G. Kandlikar, A general correlation for saturated two-phase flow boiling heat transfer inside horizontal and vertical tubes, J. Heat Transf. 112 (1) (1990) 219–228, https://doi.org/10.1115/1.2910348.

[28] G.M. Lazarek, S.H. Black, Evaporative heat transfer, pressure drop and critical heat flux in a small vertical tube with R-113, Int. J. Heat Mass Transf. 25 (7) (1982) 945–960, https://doi.org/10.1016/0017-9310(82)90070-9.

[29] L. Cheng, G. Ribatski, J.R. Thome, New prediction methods for CO_2 evaporation inside tubes: Part II—an updated general flow boiling heat transfer model based on flow patterns, Int. J. Heat Mass Transf. 51 (1–2) (2008) 125–135, https://doi.org/10.1016/j.ijheatmasstransfer.2007.04.001.

[30] S.L. Qi, P. Zhang, R.Z. Wang, L.X. Xu, Flow boiling of liquid nitrogen in micro-tubes: Part II–Heat transfer characteristics and critical heat flux, Int. J. Heat Mass Transf. 50 (25–26) (2007) 5017–5030, https://doi.org/10.1016/j.ijheatmasstransfer.2007.08.017.

[31] W.H. McAdams, W.E. Kennel, C.S. Minden, R. Carl, P.M. Picornell, J.E. Dew, Heat transfer at high rates to water with surface boiling, Ind. Eng. Chem. 41 (9) (1949) 1945–1953, https://doi.org/10.1021/ie50477a027.

[32] J.R.S. Thorn, W.M. Walker, T.A. Fallon, G.F.S. Reising, Boiling in sub-cooled water during flow up heated tubes or annuli, Proc. Inst. Mech. Eng. Conf. Proc. 180 (3) (1965) 226–246, https://doi.org/10.1243/PIME_CONF_1965_180_117_02.

[33] W.H. Jens, P.A. Lottes, Analysis of heat transfer, burnout, pressure drop and density date for high-pressure water, Report No. ANL-4627, Lemont, IL, USA, 1951.

[34] S. Seyedzadeh, F.P. Rahimian, I. Glesk, M. Roper, Machine learning for estimation of building energy consumption and performance: a review, Vis. Eng. 6 (1) (2018) 5, https://doi.org/10.1186/s40327-018-0064-7.

[35] H.U. Cho, Y. Nam, E.J. Choi, Y.J. Choi, H. Kim, S. Bae, J.W. Moon, Comparative analysis of the optimized ANN, SVM, and tree ensemble models using Bayesian optimization for predicting GSHP COP, J. Build. Eng. 44 (2021), 103411, https://doi.org/10.1016/j.jobe.2021.103411.

[36] Z. Liu, I.A. Karimi, Gas turbine performance prediction via machine learning, Energy 192 (2020), 116627, https://doi.org/10.1016/j.energy.2019.116627.

[37] M. Aliramezani, C.R. Koch, M. Shahbakhti, Modeling, diagnostics, optimization, and control of internal combustion engines via modern machine learning techniques: A review and future directions, Progress in Energy and Combustion SciencEProg. Energy Combust. Sci. 88 (2022), 100967, https://doi.org/10.1016/j.pecs.2021.100967.

[38] M. Ghalandari, M. Irandoost Shahrestani, A. Maleki, M. Safdari Shadloo, M. El Haj Assad, Applications of intelligent methods in various types of heat exchangers: a review, Journal of Thermal Analysis and CalorimetryJ. Therm. Anal. Calorim. 145 (4) (2021) 1837–1848, https://doi.org/10.1007/s10973-020-10425-3.

[39] K. Kim, H. Lee, M. Kang, G. Lee, K. Jung, C.R. Kharangate, M. Asheghi, K. E. Goodson, H. Lee, A machine learning approach for predicting heat transfer characteristics in micro-pin fin heat sinks, Int. J. Heat Mass Transf. 194 (2022), 123087, https://doi.org/10.1016/j.ijheatmasstransfer.2022.123087.

[40] T. Ma, Z. Guo, M. Lin, Q. Wang, Recent trends on nanofluid heat transfer machine learning research applied to renewable energy, Renew. Sustain. Energy Rev. 138 (2021), 110494, https://doi.org/10.1016/j.rser.2020.110494.

[41] H. Wei, H. Bao, X. Ruan, Machine learning prediction of thermal transport in porous media with physics-based descriptors, Int. J. Heat Mass Transf. 160 (2020), 120176, https://doi.org/10.1016/j.ijheatmasstransfer.2020.120176.

[42] S. Guanghui, K. Morita, K. Fukuda, M. Pidduck, J. Dounan, J. Miettinen, Analysis of the critical heat flux in round vertical tubes under low pressure and flow oscillation conditions. applications of artificial neural network, Nucl. Eng. Des. 220 (1) (2003) 17–35, https://doi.org/10.1016/S0029-5493(02)00304-7.

[43] W.J. Wang, L.X. Zhao, C.L. Zhang, Generalized neural network correlation for flow boiling heat transfer of R22 and its alternative refrigerants inside horizontal smooth tubes, Int. J. Heat Mass Transf. 49 (15–16) (2006) 2458–2465, https://doi.org/10.1016/j.ijheatmasstransfer.2005.12.021.

[44] T. Cong, R. Chen, G. Su, S. Qiu, W. Tian, Analysis of CHF in saturated forced convective boiling on a heated surface with impinging jets using artificial neural network and genetic algorithm, Nucl. Eng. Des. 241 (9) (2011) 3945–3951, https://doi.org/10.1016/j.nucengdes.2011.07.029.

[45] S. Zaidi, Novel application of support vector machines to model the two phase boiling heat transfer coefficient in a vertical tube thermosiphon reboiler, Chem. Eng. Res. Des. 98 (2015) 44–58, https://doi.org/10.1016/j.cherd.2015.04.002.

[46] Y. Qiu, D. Garg, L. Zhou, C.R. Kharangate, S.M. Kim, I. Mudawar, An artificial neural network model to predict mini/micro-channels saturated flow boiling heat transfer coefficient based on universal consolidated data, Int. J. Heat Mass Transf. 149 (2020), 119211, https://doi.org/10.1016/j.ijheatmasstransfer.2019.119211.

[47] G.A. Longo, S. Mancin, G. Righetti, C. Zilio, L. Ortombina, M. Zigliotto, Application of an artificial neural network (ANN) for predicting low-GWP refrigerant boiling heat transfer inside brazed plate heat exchangers (BPHE), Int. J. Heat Mass Transf. 160 (2020), 120204, https://doi.org/10.1016/j.ijheatmasstransfer.2020.120204.

[48] U. Sajjad, I. Hussain, K. Hamid, S.A. Bhat, H.M. Ali, C.C. Wang, A deep learning method for estimating the boiling heat transfer coefficient of porous surfaces, Journal of Thermal Analysis and CalorimetryJ. Therm. Anal. Calorim. 145 (4) (2021) 1911–1923, https://doi.org/10.1007/s10973-021-10606-8.

[49] L. Zhou, D. Garg, Y. Qiu, S.M. Kim, I. Mudawar, C.R. Kharangate, Machine learning algorithms to predict flow condensation heat transfer coefficient in mini/micro-channel utilizing universal data, Int. J. Heat Mass Transf. 162 (2020), 120351, https://doi.org/10.1016/j.ijheatmasstransfer.2020.120351.

[50] G. Zhu, T. Wen, D. Zhang, Machine learning based approach for the prediction of flow boiling/condensation heat transfer performance in mini channels with serrated fins, Int. J. Heat Mass Transf. 166 (2021), 120783, https://doi.org/10.1016/j.ijheatmasstransfer.2020.120783.

[51] E. Cho, H. Lee, M. Kang, D. Jung, G. Lee, S. Lee, C.R. Kharangate, H. Ha, S. Huh, H. Lee, A neural network model for free-falling condensation heat transfer in the presence of non-condensable gases, Int. J. Therm. Sci. 171 (2022), 107202, https://doi.org/10.1016/j.ijthermalsci.2021.107202.

[52] F. Nie, H. Wang, Y. Zhao, Q. Song, S. Yan, M. Gong, A universal correlation for flow condensation heat transfer in horizontal tubes based on machine learning, Int. J. Therm. Sci. 184 (2023), 107994, https://doi.org/10.1016/j.ijthermalsci.2022.107994.

[53] Y. Qiu, T. Vo, D. Garg, H. Lee, C.R. Kharangate, A systematic approach to optimization of ANN model parameters to predict flow boiling heat transfer coefficient in mini/micro-channel heatsinks, Int. J. Heat Mass Transf. 202 (2023), 123728, https://doi.org/10.1016/j.ijheatmasstransfer.2022.123728.
[54] C.R. Kharangate, L.E. O'Neill, I. Mudawar, Effects of two-phase inlet quality, mass velocity, flow orientation, and heating perimeter on flow boiling in a rectangular channel: Part 1–Two-phase flow and heat transfer results, Int. J. Heat Mass Transf. 103 (2016) 1261–1279, https://doi.org/10.1016/j.ijheatmasstransfer.2016.05.060.
[55] L.E. O'Neill, I. Mudawar, M.M. Hasan, H.K. Nahra, R. Balasubramaniam, N.R. Hall, A. Lokey, J.R. Mackey, Experimental investigation into the impact of density wave oscillations on flow boiling system dynamic behavior and stability, Int. J. Heat Mass Transf. 120 (2018) 144–166, https://doi.org/10.1016/j.ijheatmasstransfer.2017.12.011.
[56] V.S. Devahdhanush, S.J. Darges, I. Mudawar, H.K. Nahra, R. Balasubramaniam, M. M. Hasan, J.R. Mackey, Flow visualization, heat transfer, and critical heat flux of flow boiling in Earth gravity with saturated liquid-vapor mixture inlet conditions–In preparation for experiments onboard the International Space Station, Int. J. Heat Mass Transf. 192 (2022), 122890, https://doi.org/10.1016/j.ijheatmasstransfer.2022.122890.
[57] J. Sjöberg, Q. Zhang, L. Ljung, A. Benveniste, B. Delyon, P.Y. Glorennec, H. Hjalmarsson, A. Juditsky, Nonlinear black-box modeling in system identification: a unified overview, Automatica 31 (12) (1995) 1691–1724, https://doi.org/10.1016/0005-1098(95)00120-8.
[58] I.A. Basheer, M. Hajmeer, Artificial neural networks: fundamentals, computing, design, and application, J. Microbiol. Methods 43 (1) (2000) 3–31, https://doi.org/10.1016/S0167-7012(00)00201-3.
[59] O.I. Abiodun, A. Jantan, A.E. Omolara, K.V. Dada, N.A. Mohamed, H. Arshad, State-of-the-art in artificial neural network applications: A survey, Heliyon 4 (11) (2018) E00938, https://doi.org/10.1016/j.heliyon.2018.e00938.
[60] W.S. McCulloch, W. Pitts, A logical calculus of the ideas immanent in nervous activity, The Bulletin of Mathematical BiophysicsBull. Math. Biophys. 5 (4) (1943) 115–133, https://doi.org/10.1007/BF02478259.
[61] A.D. Rasamoelina, F. Adjailia, P. Sincak, A review of activation function for artificial neural network, in: Proceedings of the 2020 IEEE 18th World Symposium on Applied Machine Intelligence and Informatics (SAMI), Herlany, Slovakia, IEEE, 2020, pp. 281–286, https://doi.org/10.1109/SAMI48414.2020.9108717.
[62] A. Krizhevsky, I. Sutskever, G.E. Hinton, ImageNet classification with deep convolutional neural networks, Communications of the ACMCommun. ACM 60 (6) (2017) 84–90, https://doi.org/10.1145/3065386.
[63] D.E. Rumelhart, G.E. Hinton, R.J. Williams, Learning representations by back-propagating errors, Nature Nature 323 (6088) (1986) 533–536, https://doi.org/10.1038/323533a0.
[64] D.P. Kingma, J. Ba, Adam: A method for stochastic optimization, (2014). http://arxiv.org/abs/1412.6980.
[65] S. Ray, A quick review of machine learning algorithms, in: Proceedings of the 2019 International Conference on Machine Learning, Big Data, Cloud and Parallel Computing (COMITCon), 2019, pp. 35–39, https://doi.org/10.1109/COMITCon.2019.8862451. Int. Conf. Mach. Learn. Big Data, Cloud Parallel ComputIEEE,.
[66] S.G. Kandlikar, Development of a flow boiling map for subcooled and saturated flow boiling of different fluids inside circular tubes, J. Heat Transf. 113 (1) (1991) 190–200, https://doi.org/10.1115/1.2910524.
[67] S.S. Papell, Subcooled boiling heat transfer under forced convection in a heated tube, NASA technical Note D-1583, Cleveland, OH, USA, 1963.
[68] M. Badiuzzaman, Correlation for subcooled boiling data, Pak. Eng. 7 (1967) 759–764.
[69] M.M. Shah, New correlation for heat transfer during subcooled boiling in plain channels and annuli, Int. J. Therm. Sci. 112 (2017) 358–370, https://doi.org/10.1016/j.ijthermalsci.2016.10.016.
[70] T.N. Tran, M.W. Wambsganss, D.M. France, Small circular- and rectangular-channel boiling with two refrigerants, Int. J. Multiph. Flow 22 (3) (1996) 485–498, https://doi.org/10.1016/0301-9322(96)00002-X.
[71] W. Li, Z. Wu, A general correlation for evaporative heat transfer in micro/mini-channels, Int. J. Heat Mass Transf. 53 (9–10) (2010) 1778–1787, https://doi.org/10.1016/j.ijheatmasstransfer.2010.01.012.
[72] X. Fang, Q. Wu, Y. Yuan, A general correlation for saturated flow boiling heat transfer in channels of various sizes and flow directions, Int. J. Heat Mass Transf. 107 (2017) 972–981, https://doi.org/10.1016/j.ijheatmasstransfer.2016.10.125.
[73] V.S. Devahdhanush, I. Mudawar, Critical heat flux of confined round single jet and jet array impingement boiling, Int. J. Heat Mass Transf. 169 (2021) 12–14, https://doi.org/10.1016/j.ijheatmasstransfer.2020.120857.
[74] H.J. Seltman, Experimental Design and Analysis, Department of Statistics, Carnegie Mellon University, 2018. https://www.stat.cmu.edu/~hseltman/309/Book/Book.pdf.
[75] The MathWorks Inc., Deep Learning Toolbox version: 14.5 (R2022b), (2022). https://www.mathworks.com.
[76] K. He, X. Zhang, S. Ren, J. Sun, Delving deep into rectifiers: Surpassing human-level performance on ImageNet classification, in: Proceedings of the 2015 IEEE International Conference on Computer Vision (ICCV), IEEE, 2015, pp. 1026–1034, https://doi.org/10.1109/ICCV.2015.123.
[77] W.A. Arnold, T.G. Hartman, J. McQuillen, Chemical characterization and thermal stressing studies of perfluorohexane fluids for space-based applications, J. Spacecr. Rocket. 44 (1) (2007) 94–102, https://doi.org/10.2514/1.22537.
[78] A. Cioncolini, L. Santini, M.E. Ricotti, Effects of dissolved air on subcooled and saturated flow boiling of water in a small diameter tube at low pressure, Exp. Therm. Fluid Sci. 32 (1) (2007) 38–51, https://doi.org/10.1016/j.expthermflusci.2007.01.007.